Biochemical and Microscopic Characterization of INFT-1: an Inverted Formin in *C. elegans*

Ying Li

Thesis submitted to the faculty of Virginia Polytechnic Institute and State University in partial fulfillment of the requirement for the degree of

Master of Science

in

Biological Sciences

Jeffrey Kuhn (Chair)

Daniel Capelluto

Liwu Li

Richard Walker

March 14 2011

Blacksburg VA

Keywords: actin, formin, profilin, nucleation, elongation, processivity

Abstract

Formins are potent regulators of actin dynamics that can remodel the actin cytoskeleton to control cell shape, cell cytokinesis, and cell morphogenesis. The defining feature of formins is the formin homology 2 (FH2) domain (Paul and Pollard, 2008), which promotes actin filament assembly while processively moving along the polymerizing filament barbed end. INFT-1 is one of six formin family members present in *Caenorhabditis elegans* (Hunt-Newbury et al., 2007) and is most closely related to vertebrate INF2, an inverted formin with regulatory domains in the C- rather than N-terminus. Nematode INFT-1 contains both formin homology 1 (FH1) and formin homology 2 (FH2) domains. However, it does not share the regulatory N-terminal Diaphanous Inhibitory Domain (DID) domain and C-terminal Diaphanous Autoregulatory Domain (DAD) domain found in mammalian INF2. In contrast to mammalian INF2, the sequence of INFT-1 starts immediately at FH1 domain and C-terminal region of INFT-1 shares little homology with INF2, suggesting that elegans INFT-1 is regulated by other mechanisms. We used fluorescence spectroscopy to determine the effect of INFT-1 FH1FH2 on actin assembly and total internal reflection fluorescence microscopy to investigate how INFT-1 formin homology 1 and formin homology 2 domains (FH1FH2) mediate filament nucleation and elongation. INFT-1 FH1FH2 nucleates actin filament and promote actin assembly. However, INFT-1 FH1FH2 reduces filament barbed-end elongation rates in the absence or presence of profilin. Evidences demonstrated that INFT-1 is non-processive, indicating a unique mechanism of nucleation. INFT-1 nucleation

efficiency is similar to the efficiency of *Arabidopsis* FORMIN1 (AFH1), another non-processive formin. High phosphate affected the assembly activity of INFT-1 FH1FH2 in the absence or presence of profilin. INFT is thus the second example of a non-processive formin member and will allow a more detailed understanding of the mechanistic difference between processive and non-processive formins.

Acknowledgement

I would like to thank my advisor Dr. Jeff Kuhn and all my committee members, Dr. Daniel Capelluto, Dr. Liwu Li, and Dr. Richard Walker. This thesis could not have been written without Dr. Jeff Kuhn who not only served as my supervisor but also encouraged and challenged me throughout my academic program. He and the other committee members, Dr. Daniel Capelluto, Dr. Liwu Li, and Dr. Richard Walker, guided me during my master education and through my thesis process. I thank them all.

I am indebted to my parents Weijun Li and Fengqin Huang. They support me all the time. I owe them a lot. I just want to say thank you and I really miss you. I also owe a debt to my boyfriend Tong Liu who helped me through the hardest time before graduation.

I also want to thank all the past and present Kuhn lab members, especially Brent, Xiaohua, Sihui and Namisha. They gave me advice and constructive criticism for my work. We had a good time working together. I will miss them all.

Table of contents

Biochemical and Microscopic Characterization of INFT-1: an Inverted Formin in *C. elegans* i

Abstract ii

Acknowledgement iv

Table of contents v

Abbreviation ix

Chapter 1 1

Literature Review 2

Introduction 2

Classification and Domain Structures of formins 4

Formins in actin bundling 5

Formins in Cytokinesis 7

Formins in Cell adhesion and motility 8

Formins in Cell polarity 11

Formins in Morphogenesis 12

Structure of the Formin FH2 domain 13

The FH2 Domain Nucleates and Assembles Actin Filaments 14

Non-processive formin 18

Profilin-FH1 interaction and Actin filament elongation 18

Regulatory mechanisms of formins 20

Chapter 2 28

Research Plan....29
Background....29
Inverted Formins....29
Formins in C. elegans....30
INFT-1 – an Inverted Formin Potentially Involved in Cell Motility....31
Material and Methods....33
Plasmid constructs:....33
Actin purification and modification....35
Expression and Purification of Profilins and INFT-1....38
Pyrene actin polymerization by fluorescence spectroscopy....41
Nucleation Efficiency Data Analysis....41
Total Internal Reflection Fluorescence (TIRF) Microscopy....42
Filament growth rate measurement....42
Statistics Analysis....43
Results....44
Cloning of C. elegans INFT-1....44
Purification of C. elegans inverted formin INFT-1 FH1FH2 domain....45
C. elegans inverted formin INFT-1 assembles actin filaments....47
INFT-1 slightly reduces the actin barbed end elongation rate....48
The actin assembly rate mediated by INFT-1 decreased in the presence of profilin....49
INFT-1 is a non-processive formin....51

INFT-1 binds to filament sides and pointed ends. 55

Nucleotide state influences filament barbed end elongation rate 56

Discussion 60

References 84

Figure contents vii

Figure 1 Formins share a conserved formin homology 2 (FH2) actin polymerizing domain along with different regulatory regions. 23

Figure 2. The FH2 Domain is a tethered dimer. 24

Figure 3 FH1FH2 dimer of processive formins nucleate actin filaments and stay at the filament barbed end as it elongates 25

Figure 4 FH2 dimer moves processively at filament barbed end through the cooperation of the two FH2 monomers and actin subunits 26

Figure 5. Diaphanous-related formins are regulated by autoinhibition 27

Figure 6 PCR amplification of full length INFT-1, INFT-1 FH1FH2 domains, and INFT-1 C-terminus. 67

Figure 7 Full-length INFT-1, INFT-1 FH1-FH2 and INFT-1 C-terminus genes were ligated into a modified pET21a vector 68

Figure 8 INFT-1 gene sequence. 69

Figure 9 INFT-1 FH1FH2 is purified through a series of chromatography. 70

Figure 10 INFT-1 FH1FH2 nucleates actin polymerization. 72

Figure 11 INFT-1 FH1FH2 dimer enhances Oregon green actin nucleation. 74

Figure 12 INFT-1 FH1FH2 slightly slows down barbed end growth rate in the

absence of presence of Ce PFN-1. 76

Figure 13. INFT-1 is a non-processive formin. 77

Figure 14: Actin bundles form around MBP-INFT-1 FH1FH2 coated spherical beads. 79

Figure 15 INFT-1 FH1FH2 mediated actin assembly is affected by excess phosphate. 81

Figure 16 INFT-1 FH1FH2 has a greater effect on slowing down barbed end growth in the presence of excess phosphate. 83

Table contents viii

Table 1: Six *C. elegans* formins. 31

Abbreviation

AFH1: *Arabidopsis* FORMIN1

CC: coiled coil

DD: dimerizaton domain

DAD: Diaphanous Autoregulatory Domain

DID: Diaphanous Inhibitory Domain

FH: formin homology

FSI: formin–Spire interaction domain

GBD: GTPase binding domain

INF: inverted formin

INFT-1: inverted formin three related 1

PDZ: Postsynaptic density protein, Discs large, Zona occludens 1 domain

WH2: WASP homology 2 domain

TIRFM: Total internal reflection fluorescence microscopy

Chapter 1

Literature Review

Introduction

Several cellular processes, such as cytokinesis, cell migration, generation of cell polarity, and morphogenesis require remodeling of actin cytoskeleton. Actin polymerization and depolymerization are thus basic processes involved in normal cellular function. The addition of actin monomers onto existing filament ends is a thermodynamically favorable process. However, the rate-limiting step, spontaneous nucleation of actin filaments, is inefficient under cellular conditions and requires specific actin nucleators to initiate polymerization. Two universal actin nucleators, Arp2/3 and formin, have been found along with other nucleators such as Spire, Cordon-bleu, Leiomodin, junction-mediating and regulatory protein (JMY), which are expressed in specific cell types (Chhabra and Higgs, 2006; Kobielak et al., 2004; Otomo et al., 2005b; Pring et al., 2003; Shimada et al., 2004; Pollard 2007; Renault, 2008; Chereau, 2008; Zuchero, 2009). Despite their similar potency in promoting actin nucleation, each nucleator generates new ends *via* a different mechanism.

Each actin monomer has a cleft on one side, which is the binding site for ATP. In an actin filament, all the actin subunits orient with their cleft in the same direction. Thus, the actin filament has polarity. Decorating actin filament with myosin "S1" fragments and observing the arrowhead pattern of S1 fragments with electron microscopy can be used to determine filament polarity. The end that most closely resembles an arrowhead is termed the pointed end and the other end is called the barbed end. Filament growth at the barbed end exceeds the growth at the pointed end.

Unlike the pointed end nucleators Arp2/3 and Spire, formins are actin barbed-end nucleators. The first member of formin family was identified in mouse and was named for the mouse gene *limb deformity* (Woychik et al., 1990). Although a later study showed that the limb defects were caused by disruption of another gene (Zuniga et al., 2004), the name formin has remained since formins play an important role in actin filament "formation". Subsequently, different formins have been identified throughout a wide range of species including animals, plants, fungi, and protists (Higgs and Peterson, 2005; Rivero et al., 2005; Wallar and Alberts, 2003). In multi-cellular organisms, formins are ubiquitously expressed in different cell types. As a result, formins are universally present in eukaryotic cells, where they are of particular importance in a variety of cellular events.

The nucleators Arp2/3 and Spire promote only limited growth of actin filaments because subsequent barbed end elongation is rapidly halted by binding of capping protein. Formins, however, compete with capping protein for binding to the barbed end and can prevent capping of growing barbed ends. Accordingly, formins can generate long actin filaments in the presence of capping protein (Harris et al., 2004; Kozlov and Bershadsky, 2004; Moseley et al., 2004). Formins nucleate linear, unbranched filaments, thus they are capable of directing distinct cellular structures containing linear unbranched actin filaments such as actin cables, stress fibers, filopodia, actin-rich cell adhesions, and cytokinetic actin rings.

Classification and Domain Structures of formins

The defining feature of all formin family proteins is their highly conserved Formin Homology 2 (FH2) domain of approximately 400 amino acid residues that is essential for actin assembly. Bioinformatics analyses of FH2 domains reveal that most eukaryotic species possess multiple formin genes, while some plants species have more than 20 formins (Higgs and Peterson, 2005; Rivero et al., 2005; Wallar and Alberts, 2003; Grunt et al, 2008; Chesarone et al, 2010). Metazoan formins segregate into seven groups by phylogenetic analysis of the FH2 domain: Dia (diaphanous formin); DAAM (disheveled-associated activator of morphogenesis); FMN (formin); FHOD (formin-homology domain containing protein); FRL (formin-related gene in leukocytes); INF (inverted formin); and Delphin. Nonmetazoan formin homology 2 domains are phylogenetically distinct from these groups, with yeast FH2 domains particularly divergent.

Other than barbed-end binding FH2 domain, almost all formins have an FH1 domain containing one or more profilin binding sites just N-terminal to FH2 domain. Figure 1 shows the domain organization of different formin members (Campellone and Welch, 2010). Although FH1 and FH2 domains are conserved among different formin classes, formins diverge considerably outside of these two regions.

The diaphanous-related formins (DRFs) are the best characterized of the formin subfamilies. DRFs include Dia, DAAM, and FRL in mammals and Bni1, Bnr1, and sepA in yeast and DRFs are effectors of Rho family GTPases (Wasserman, 1998). In DRFs, the FH1 and FH2 domains are flanked by several N-terminal regulatory

domains and a single C-terminal diaphanous-autoregulatory domain (DAD) (Alberts, 2001). The C-terminal DAD domain is composed of a short segment of approximately 17 amino acid residues immediately following the FH1 and FH2 domains. The C terminal FH1-FH2 domains of a DRF are crucial for actin assembly, whereas the N-terminal serves primarily as an auto-regulatory region that interacts with the C terminal active half to keep formins in an autoinhibited state (Alberts, 2001; Watanabe et al., 1999). The N terminal autoregulatory region contains four domains: the GTPase binding domain (GBD); (Albertson et al., 2001), the diaphanous inhibitory domain (DID), the dimerization domain (DD), and a coiled-coil region (CC) (Figure 1) that bind to specific upstream regulators.

In addition to DRFs, more divergent formin groups such as INF (inverted formin) and Delphilin do not possess an obvious GBD domain. Inverted formins group are so called because their regulatory domains are C-terminal to their active domains, and their FH1 and FH2 domain are at the N-terminus rather than in C-terminal region (Goode and Eck, 2007). Delphinlin does not contain DID, and DD domains, either (Miyagi et al, 2002; Matsuda, 2006). Moreover, all the plant formins characterized to date have neither GBD, DID, nor DD domains (Grunt et al, 2008).

Formins in actin bundling

Actin filaments can be crosslinked by proteins that contain two actin binding motifs such as α-actinin or proteins with one actin binding motif that form obligate homodimers. When actin crosslinkers have high affinity binding to filaments and

short inter-binding domains, they form actin bundles or actin cables. Actin bundles are important in providing cell shape, cell support, and cell movement. Recent study shows that several formins, including mouse FRL1 and mDia2, yeast Bnr1, and *Arabidopsis* FORMIN1 (AFH1), can bundle actin filaments (Harris, 2006; Moseley, 2005; Michelot, 2006). All the four formins above are able to bind the side of actin filaments. FRL1 and AFH1 have high affinity to the side of the actin filaments, with a $K_d \sim 0.1$ μM (Michelot et al, 2006). Mouse mDia1, which cannot induce actin bundles, binds to actin filament side weakly with a $K_d \sim 3$ μM. High affinity might help actin bundle formation (Michelot et al, 2006) because it may increase the interaction among different actin filaments. Common actin filament side binding activity in these four formins indicates that the bundling activity of formins might be related to their side binding affinity.

Although these formins promote actin bundle formation, different domains or different regions within one domain are responsible for this activity. Mouse FRL1 and mDia2 bundle actin filaments *via* their FH2 domain (Harris, 2006; Michelot et al, 2006). The bundling activity of FRL1 competitively inhibits its barbed-end binding, suggesting that the same region in the FH2 domain is responsible for both activities. In contrast, the actin bundling and barbed-end binding activities of mouse mDia2 are independent, indicating that mDia2 separate regions are responsible for filament bundling and end binding (Harris, 2006; Michelot et al, 2006). *Arabidopsis* AFH1 requires both FH1 and FH2 domains to bind to the side of filaments and induce actin bundling, though its FH1 domain alone does not bind actin filament or monomers

(Michelot et al, 2006). The mechanisms by which these four formins (mDia2, FRL1, Bnr1 and AFH1) regulating actin bundle formation are still unclear, but they likely follow different mechanisms since different domains are responsible for bundling activities.

Formins in Cytokinesis

Cytokinesis, the separation of cytoplasm to form two daughter cells, is the final step in mitotic and meiotic cell division. In most animal cells, cytokinesis requires the formation and constriction of a cytokinetic actin ring (CAR) at the site of cell separation. Rho family GTPases play a central role in controlling this highly regulated step and function through several downstream effectors, including actin, non-muscle myosin II, and a several accessory proteins.

The first evidence for formin's function in cytokinesis was found in *Drosophila.* Flies with mutations in the formin, *diaphanous*, failed in cell division during spermatogenesis (Castrillon and Wasserman, 1994). Subsequent loss-of-function studies showed that formins are involved in cytokinesis in a wide range of organisms including vertebrates, budding and fission yeast, *Drosophila, C. elegans*, and plants. Formins invariably are essential for the formation and maintenance of CAR (Castrillon and Wasserman, 1994; Chang et al., 1997; Echard, 2004; Imamura et al., 1997; Ingouff et al., 2005; Peng et al., 2003; Severson et al., 2002; Swan et al., 1998; Tolliday et al., 2002; Tominaga et al., 2000) (Kovar, 2003; Neidt, 2009). Electron microscopy has shown that actin filaments in the CAR are organized into bundles of

predominantly linear filaments, consistent with formin's role in actin assembly. Furthermore, lost-of-function studies in *Drosophila, C. elegans*, and budding yeast have shown that the formation of CAR and cytokinesis are unaffected by loss of the Arp2/3 complex, indicating the specialized actin filaments in CAR are nucleated by formins rather than by Arp2/3 (Tominaga et al., 2000). The formation of actin contractile ring in fission yeast requires formin Cdc12p to assemble actin filaments. A recent review by Thomas Pollard summarized a model to explain the assembly of the contractile ring in fission yeast in details (Paul and Pollard, 2008). Roughly 65 nodes, which contain myosin-II and formin Cdc12p, form around the cell equator in fission yeast. Actin starts to polymerize into filaments at these nodes and this polymerization is mediated by Cdc12p in fission yeast. Myosin-II captures actin filaments from adjacent nodes and pulls them together, condensing actin filament and associated nucleation nodes into a focused contractile ring (Paul and Pollard, 2008).

Formins in Cell adhesion and motility

Dynamic rearrangement of the actin cytoskeleton is essential for cell migration and cell-cell and cell-substrate adhesion. Cytoskeletal rearrangements give rise to dramatic cell shape changes that include plasma membrane protrusions, formation and release of contacts with neighboring cells, and contraction of the cell body. The Arp2/3 complex promotes the assembly of highly branched actin filaments network at the leading edge to form a lamellipodium (Lu and Pollard, 2001). Lamellipodia can develop filopodia, long, thin cell membrane protrusions composed of parallel bundles

of unbranched actin filaments that grow by addition of actin monomers at the filopodia tips (Mallavarapu and Mitchison, 1999). Filopodia are highly dynamic structures used by many types of cell to sense their environment and guide cell migration and axon extension (Peng et al., 2003; Severson et al., 2002).

Formins are implicated in filopodia assembly. RNA interference (RNAi) studies showed that Arp2/3 may not be required for the formation of filopodia (Steffen et al., 2006). In *Dictyostelium*, GFP-tagged as well as endogenous dDia2 accumulated at the distal tips of filopodia, and gene disruption of dDia2 impaired filopodia formation (Schirenbeck et al., 2005b). These findings suggest that Dia localizes to the tips of filopodia and plays a significant role in filopodia formation in multiple species (Pellegrin and Mellor, 2005; Peng et al., 2003; Schirenbeck et al., 2005b).

The filopodial tip complex also contains Ena/VASP proteins. Ena/VASP proteins were proposed to protect actin filament barbed ends from capping protein (Schirenbeck et al., 2005a). Ena/VASP is required for filopodia formation in *Dictyostelium* (Schirenbeck et al., 2005a). Thus, Ena/VASP, like formins, may promote the growth of long filaments filopodia (Evangelista et al., 2002; Nakano et al., 1999; Sagot et al., 2002a). Considering the similarities in function and localization, further studies on whether formin and Ena/VASP work together to form filopodia and how each contributes to filopodia formation *in vivo* are needed.

Formins and their upstream Rho activators play essential roles in the assembly of cell adhesion junctions and stress fibers. In mammalian epithelia, adherens junction complexes containing E-cadherins and catenins polarize epithelial cells. Mammalian

α-catenin binds to the formin-1 coiled-coil domain, recruiting it to adherens junctions (Kobielak et al., 2004). Mammalian formin-1 induces unbranched actin filament formation at the adherens junctions and promotes actin filament bundling. If the interaction between α-catenin and formin-1 is disrupted in adherens junctions, radial actin cable formation is also eliminated. Rho and formin also help assemble stress fibers, unbranched actomyosin structures that play roles in cell-substrate adhesion and retraction during cell migration. Truncated mDia1 lacking the N-terminal regulatory domain induced long, parallel stress fibers, suggesting mDia1 is a downstream effector of Rho in stress fiber assembly (Nakano et al., 1999; Watanabe et al., 1999). A subsequent live-cell imaging study observed several stages of stress fiber formation and showed that mDia1 helps assemble dorsal stress fibers by polymerizing actin at focal adhesions (Hotulainen and Lappalainen, 2006). Mouse mDia1 also promotes the clustering of E-cadherin and α-catenin at both cell-cell contracts and the cell periphery (Sahai and Marshall, 2002).

Formins play a role in cell migration (Nakano et al., 1999; Watanabe et al., 1999). Overexpression of FHOD1 promotes cell migration (Watanabe et al., 1999), but *Dictyostelium* amoeboid cell movement is blocked by overexpression of dDia2 (Schirenbeck et al., 2005b). The nature of Dia or FHOD1 family formin involvement in cell motility is still unclear, as is the contributions of other formin homologues. Further studies about the nature of these differences and the roles of other formin homologues are needed.

Formins in Cell polarity

Cells display different types of polarity: they exhibit apical-lateral polarity; the polarity perpendicular to the apical-lateral axis of the cells is called planar cell polarity (PCP); cells also have a front and back polarity. The leading edge is the front, and the opposite side is the back. This front-back polarity tells the cells which direction to go. If the front-back polarity is perturbed, the cells can move toward any direction which can cause problems (Schoenwaelder, 2002). The establishment of cell polarity requires the rearrangement of actin and/or microtubule cytoskeleton (Schoenwaelder, 2002), and formins participate in polarizing cells by remodeling the actin cytoskeleton. The first evidence that formins are essential for cell polarity was the study of the *Drosophila* formin cappuccino, which is required for polarity of both the egg and embryo (Emmons et al., 1995). Several formins are also required for polarized cell growth in yeast. In budding yeast, the formins Bni1p and Bnr1p are involved in polarized bud formation. Both interact with profilin to remodel the actin cytoskeleton into cable-like structures at the bud cortex (Evangelista et al., 2002; Imamura et al., 1997; Sagot et al., 2002b), and Bni1 and Bnr1 assemble different forms of actin cables from these two sites (Evangelista et al., 2002; Sagot et al., 2002a). Actin cables serve as the cargo to transfer proteins and other factors needed for bud formation from the cell body to the bud. During bud formation, Bni1 is recruited to the bud tip while Bnr1 localizes at the bud neck. They bind differentially to the cell polarity factor, Bud6 (Faix and Grosse, 2006), which directly stimulates the activity of Bni1.

In fisson yeast, the formin For3p localizes at the cell tips and facilitates actin cable assembly and polarized cell growth (Evangelista et al., 2002; Martin et al., 2005; Sagot et al., 2002a). In addition, plant formins have been demonstrated to promote actin cable assembly in pollen, indicating a role in polarized elongation of pollen tube (Cheung and Wu, 2004). Further research should elucidate whether similar mechanisms are present in mammalian systems.

Formins in Morphogenesis

Several formins are involved in morphogenesis, the process by which organism starts to develop its shape. In epithelium plane, the organization of cells is called planar cell polarity (PCP). PCP is perpendicular to apical/basal polarity. The axis along this polarity is called the planar axis. The conserved PCP pathway in Drosophila involves frizzled and disheveled signaling and regulates the integrity and orientation of cells in the planar axis. The first formin implicated in morphogenesis was identified as a novel binding partner of disheveled. Disheveled-associated activator of morphogenesis (Daam1) binds to RhoA and regulates *Xenopus* gastrulation (Habas et al., 2001). Inhibition of endogenous Daam1 protein synthesis resulted in severe gastrulation abnormalities, indicating a crucial role of Daam1 in this process (Habas et al., 2001). *Drosophila* Daam1 appears to organize actin cytoskeleton in tracheal cells of the respiratory system (Matusek et al., 2006). Furthermore, formin-3 in *Drosophila* was shown to be required for actin reorganization in tracheal development (Tanaka et al., 2004).

Structure of the Formin FH2 domain

The crystal structure of yeast Bni1 FH2 domain showed a flexible tethered dimer architecture, with an N-terminal "lasso" region surrounding a central "post" region to form the dimer (Xu et al., 2004). Further studies of three mammalian formin FH2 domains, from mDia1, mDia2 and FRL1, showed a similar dimeric structure (Harris et al., 2004; Li and Higgs, 2005) with similar architecture that is shared by all FH2 domains.

The stable FH2 dimer is composed of two rod-shaped subunits that link to form a toroidal structure with a central hole. Dimerization is required for actin assembly. Mutations that decrease dimerization eliminate actin assembly function (Xu et al., 2004). The first crystal structure of formin FH2 domain in complex with actin is reported in 2005 (Otomo et al., 2005b). In this report, the researchers determined the crystal structure of the complex with yeast Bni1p FH2 domain and tetramethylrhodamine-actin (Otomo et al., 2005b). Each FH2 subunit in the dimer is a functional actin binding head that serves as the bridge between lateral actin subunits at the barbed end (Otomo et al., 2005b; Xu et al., 2004). Each subunit also contains a flexible linker region, a knob region, a coiled-coil region and a post region (Figure 2). Together, these regions are arranged in a heat-to-tail pattern that dimerizes through lasso/post interactions, an interface that is highly conservative among all known formins (Goode and Eck, 2007) .

Interactions between actin subunits and Bni1 are made by two highly conserved

surface patches on each half of the dimer. One is on the knob region and centered on I1431, whereas the other is formed by lasso and post region and centered on K1601. Mutation of either abolishes the actin assembly activity (Xu et al., 2004). The donut-shaped circular structure of FH2 dimer along with the flexible linker regions allows the dimer to expand and contract to processively step along growing actin filament barbed ends.

The FH2 Domain Nucleates and Assembles Actin Filaments

Actin filament assembly is a multi-step process, consisting of an unfavorable filament nucleation step followed by a fast elongation step (Pollard and Cooper, 1986). In cells, profilin bound to free actin further inhibits spontaneous filament nucleation. Therefore, cells use a small suite of nucleating proteins and complexes to tightly regulate filament nucleation. The first evidence for the importance of formins to nucleation was that the FH2 domain of Bni1 is crucial for actin assembly in *vivo* in a Bnr1 null background in budding yeast. (Evangelista et al., 2002; Sagot et al., 2002a). Formin FH2 domains have been shown to influence actin assembly in different ways including promoting actin nucleation, affecting actin polymerization and depolymerization rates, and preventing filament barbed-end capping by capping proteins (Figure 3). The rate limiting steps in *de novo* actin nucleation are dimer and trimer formation, steps that are also inhibited by profilin binding. Although dimers and trimers form in solution, they rapidly fall apart. Unlike the other major actin nucleator, Arp2/3, formin FH2 domains are not structurally similar to actin and do not

mimic actin filaments. However, studies including kinetic modeling suggest that the formin FH2 dimer directly interacts with and stabilizes actin dimers or trimers to create filament nuclei (Figure 3) (Higgs, 2005; Otomo et al., 2005b; Pring et al., 2003; Shimada et al., 2004; Xu et al., 2004). Formin nucleation produces unbranched actin filaments with formins associated at their barbed ends. Studies on the biochemical effects of the FH2 domain showed that nanomolar concentrations of purified Bni1 FH2 and longer fragments including both FH1 and FH2 domains induced actin nucleation (Pruyne et al., 2002; Sagot et al., 2002b). Consistent with Bni1, FH2 and FH1-FH2 fragments from most formin species have nucleating activities, with the exception of Delphilin and FHOD (Chhabra and Higgs, 2006; Harris et al., 2004; Kobielak et al., 2004; Li and Higgs, 2003; Moseley et al., 2004).

The FH2 domain is also important for filament elongation. Using cytochalsins B and D to "block" pointed end elongation, studies on Bni1 FH2 and FH1-FH2 showed that Bni1 FH2 and FH1-FH2 nucleated filaments elongated at their barbed ends (Pruyne et al., 2002; Sagot et al., 2002b). Another study showed that the Bni1 nucleated filaments still grew after blocking pointed end elongation by high concentration of profilin, supporting the notion that formins promote barbed end elongation (Sagot et al., 2002b). Immunogold labeling and direct observation from electron microscopy also demonstrated that Bni1 associated with filament barbed end (Pruyne et al., 2002). Furthermore, when filament barbed ends were saturated with Bni1, the elongation rate is still 50% of the normal elongation rate. These studies showed that barbed ends capped by Bni1 FH2 domains can still elongate. FH2

domains from other formins, including mDia1, mDia2, Bnr1, INF2, have also been shown to allow barbed-end elongation, but the elongation rates permitted by different FH2 domains vary by 5- to 10-fold (Kovar et al., 2006).

The observation that Bni1 remained at the barbed end lead to the "stair step" hypothesis: that Bni1 processively moves at the filament barbed end. The first evidence for processive movement of FH2 domains along growing filament barbed ends was made by Pruyne and colleagues (Pruyne et al., 2002). They found that Bni1p FH1FH2 domain remained bound to the barbed end of actin filaments. Other studies showed that FH2 domains protect elongating barbed ends capping by vast molar excesses of capping protein (Harris et al., 2004; Moseley et al., 2004; Zigmond et al., 2003). So far, the most convincing evidence for processive movement of formins has come from TIRF microscopy studies of individual, growing actin filaments. Purified formins immobilized on a glass surface nucleated actin filaments whose growth was monitored by TIRF microscopy (Kovar and Pollard, 2004). Filaments grew away from the surface while their growing barbed ends remained attached to individual formins on the surface. This study conclusively demonstrated that formins persistently associated with filament barbed end.

Several models for FH2-mediated elongation and processive movement have been proposed (Harris et al., 2004; Kozlov and Bershadsky, 2004; Moseley et al., 2004; Otomo et al., 2005b; Xu et al., 2004). However, the most comprehensive model (Figure 4) was put forth by Good and Eck and integrates several previous models with previous studies and available structural information (Goode and Eck, 2007). In

processive movement, the two FH2 subunits work as the bridge during polymerization or depolymerization. During barbed end elongation, each FH2 subunit alternates between a “bound” state and a “migrating” state. The bound bridge interacts tightly with the terminal and penultimate actin subunits at barbed end. The terminal subunit is in a straightened, 180º strained orientation rather than the more relaxed 166º helical “actin filament” orientation that is required for tight lateral subunit binding and gives actin filament its twist.

The migrating bridge binds weakly and allows the addition or dissociation of an actin subunit. The migrating bridge can be described in equilibrium between two configurations: open or closed, also described as “down” or “up” positions respectively in references to the canonical depiction of an actin filament with barbed end facing downward. In the open configuration, the migrating bridge is in the “down” position binding the ultimate actin subunit with its knob region, and its post region is exposed to allow actin addition. In the closed configuration, the migrating bridge is in the “up” position and only interacts with the penultimate subunit with its post site. In this model, actin subunit addition occurs when the migrating bridge is in the open configuration. The newly added actin subunit is in the strained 180º orientation and induces a conformational change of the penultimate subunit into a 166º actin filament orientation. After that, the migrating bridge interacts with newly added subunit and penultimate subunit becoming the bound bridge. Due to the conformational change, the formerly bound bridge weakly interacts with the penultimate subunit in the actin filament orientation, thus it becomes the migrating

bridge. Therefore in each cycle of actin subunit addition, the filament is one actin subunit longer and the bridges' roles are reversed.

Non-processive formin

Although most formins have been found to be processive, non-processive formins also exist. *Arabidopsis* AFH1 is the first non-processive formin found (Michelot et al, 2006). When AFH1 is immobilized on a slide, actin filaments generated by AFH1 move away from the origin where they are nucleated (Michelot et al, 2006), indicating that *Arabidopsis* AFH1 does not consistently associate with the actin filament barbed end. Thus AFH1 differs from most other formins that stay at the filament barbed end. Once it dissociates from the barbed end after nucleation, AFH1 binds to the side of the actin filament (Michelot et al, 2006) as shown by GFP labeled AFH1 protein. *Arabidopsis* AFH1 has a high affinity to the filament side with a K_d of approximately 0.1 μM. After binding to the filament side, AFH1 is still able to initiate the nucleation of new actin filaments (Michelot et al, 2006) whose barbed ends grow away from their origin (Michelot et al, 2006). *Arabidopsis* AFH1 is also shown to induce actin bundle formation while binding to actin filament side. The side binding and actin bundle activities of AFH1 are dependent on both FH1 and FH2 domains (Michelot et al, 2006). However, the exact mechanism of *Arabidopsis* AFH1 bundling of actin filaments has not been elucidated.

Profilin-FH1 interaction and Actin filament elongation

Formin homology 1 (FH1) domains found in all formins lie N-terminal to the

FH2 domain, have high proline contents (35-100%), but are highly variable in length (15-229 residues). FH1 domains from different formins contain 1-16 poly-proline regions. Poly-proline regions that contain more than 5 prolines each can bind to the actin monomer-binding protein profilin.

In most eukaryotic cells, profilin-actin is the predominant form available for polymerization (Pollard et al., 2000). Profilin bound actin monomer is unable to nucleate or add to filament pointed ends but can add to barbed ends at similar rate as free monomer (Pollard et al., 2000). Upon barbed end polymerization, profilin rapidly dissociates, leaving a free actin subunit available for further polymerization. Therefore, profilin-actin suppresses spontaneous filament nucleation but can be used in barbed end elongation. Several studies showed that profilin binds within formin FH1 domains (Harris et al., 2004; Kovar et al., 2003; Kovar and Pollard, 2004; Li and Higgs, 2003; Pring et al., 2003; Sagot et al., 2002b). FH1 domains bind profilin *via* the poly-proline sites, and profilin can simultaneously interact with actin and an FH1 domain while remaining polymerization competent.

FH1-profilin interactions allow formin to efficiently use profilin-actin and increase the filament elongation rate. The *S. pombe* Cdc12p is the only known formin that completely caps filament barbed ends. However, total internal reflection fluorescence (TIRF) microscopic studies showed that Cdc12p FH1-FH2 nucleated filaments were able to elongate in the presence of profilin (Kovar et al., 2003). Subsequent studies by TIRF microscopy revealed that all the tested formin FH1-FH2 domains increased barbed end elongation rates, including Bni1 (Kovar and Pollard,

2004) and mDia1 (Romero et al., 2004). How then does FH1-profilin interaction affect elongation rate? There are several possibilities: (1) profilin may increase actin monomer concentration near the barbed ends; (2) formins hold profilin-actin in the correct orientation for addition to barbed end; or (3) FH2 domain processive movement rate may be changed by profilin. Although these models are not mutually exclusive, Paul and Pollard (Paul and Pollard, 2008) designed some experiments to test the first model. They created artificial formin constructs with one or more consecutive FH1 domains preceding an FH2 domain and showed that the increase in actin polymerization rate was proportional to the number of poly-proline sites (Paul and Pollard, 2008), in support of the first mechanism above.

Regulatory mechanisms of formins

In *vivo* studies indicated that members of diaphanous related formins are auto-inhibited by intramolecular interactions between the N-terminal diaphanous inhibitory domain (DID) and C-terminal diaphanous autoinhibitory domain (DAD) regions. The DID is at the N-terminus of DRFs together with GTPase binding domain (GBD) and dimerization domain (DD). In mDia1, the DID is composed of four armadillo repeats and a truncated fifth repeat. GBD and DID domains are connected by a poorly ordered loop of approximately 11 residues. DAD is a stretch of 20-30 amino acids C-terminal to the FH2 domain (Alberts, 2001; Higgs and Peterson, 2005). The DAD domain consists of a conserved core region with a consensus "MDXLLXL" sequence. The adjacent C-terminal region is variable in length but often basic. DAD

has been found to interact with the N-terminus in yeast two-hybrid (Alberts, 2001) studies and through direct biochemical interaction (Li and Higgs, 2005). Deletion of DAD in mDia1 DID-containing constructs *in vitro* led to a great decrease in inhibitory potency (Li and Higgs, 2005).

Cellular studies showed that mDia1 and mDia2 are constitutively auto-inhibited (Alberts, 2001; Watanabe et al., 1999) and that Rho-family proteins relieve this auto-inhibition. The interaction between formin mDia and RhoA GTPase is the best characterized. The model for mDia inhibition and activation is shown in Figure 5 (Campellone and Welch, 2010). The RhoA-binding region in mDia1 has been narrowed to amino acids 60-260 (Watanabe et al., 1997). DID partially overlaps with this region (Li and Higgs, 2005). The Rho and DAD binding regions in the N terminus are not overlapping from biochemical and NMR evidence (Otomo et al., 2005a; Rose et al., 2005). Comparisons of DAD/N-terminal complex and Rho/N-terminal complex showed that Rho and DAD cannot simultaneously bind. Therefore, RhoA is likely to allosterically inhibit DAD/DID binding. A number of studies of RhoA and DAD binding to the mDia1 N-terminus showed that RhoA binding is about ten-fold tighter than DAD binding (Lammers et al., 2005; Li and Higgs, 2005; Nezami et al., 2006; Rose et al., 2005). Thus RhoA is able to displace the DAD/DID autoinhibition.

Unlike DRFs, there are a growing number of formins which seem not to be regulated by DID-DAD interaction and Rho GTPases activation. These formins, including Delphilin, INF proteins, all plant formins known so far, and Cappuccino,

lack apparent GBD, DID and DAD domains (Higgs, 2005; Miyagi, 2002; Matsuda, 2006; Grunt, 2008). It is possible that they can be inhibited by other binding proteins. So far, three groups of formin binding partners have been found: Dia-interacting protein (DIP), Spire and Bud-14 (Quinlan, 2007; Eisenmann et al, 2007; Chesarone, 2009). They interact with mDia-1 and mDia-2, Cappuccino, and Bnr-1, respectively (Eisenmann, 2007; Chesarone, 2009). Thus formins are inhibited by these ligands.

Although Rho GTPases can release the autoinhibition of formins, they might require additional partners to accomplish this task. At least 8 μM of purified Rho is required to activate formins completely and accelerate actin assembly in *vitro* (Seth et al, 2006; Brandt et al, 2007), but this concentration may be too high to be practical in *vivo* (Chesarone et al, 2010). It is possible that other factors participate in formin activation in *vivo*. If there are other factors involved in formin activation, this may provide a reasonable explanation of activation for those formins who do not possess GBD, DID, and DAD. Recent studies found that disheveled, p53-regulating kinase, ROCK, and the RAC1- and Cdc42-effector IQ motif-containing GTPase activating protein (IQGAP1), etc are regulators that can activate formins alone or with Rho proteins (Seth, 2006; Wang, 2009; Brandt, 2007;).

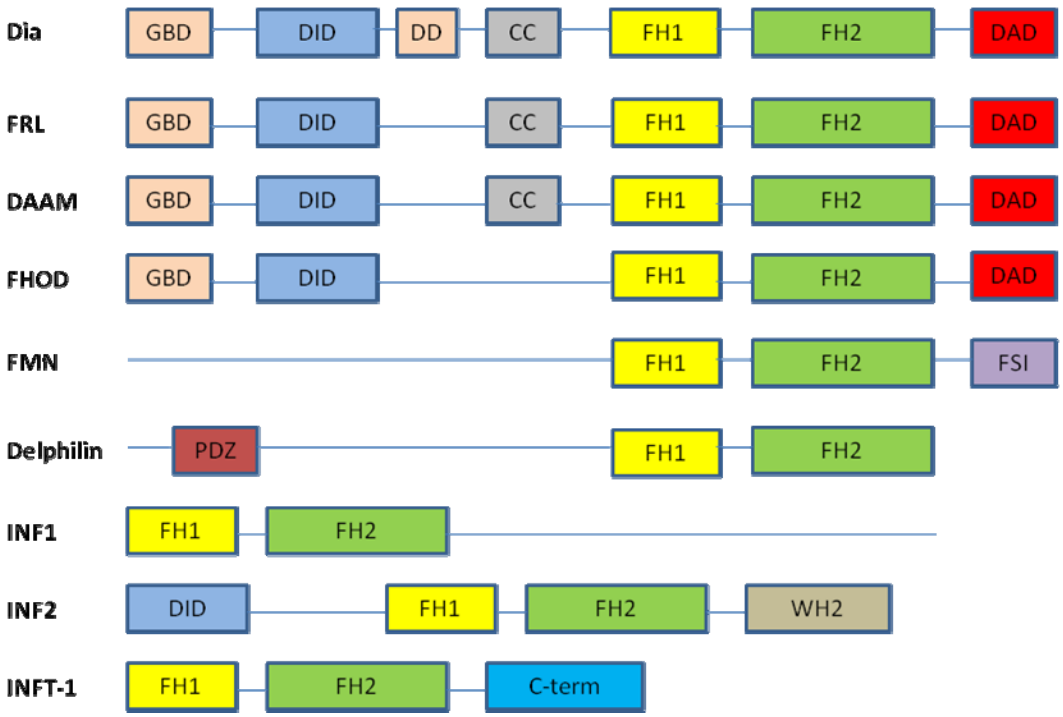

Figure 1 Formins share a conserved formin homology 2 (FH2) actin polymerizing domain along with different regulatory regions. Domain organizations of different formins, which belong to 7 different groups, are shown as above. The name of each group is indicated on the left. The last three are all from inverted formin group (adapted from Campellone and Welch, 2010). GBD: the GTPase binding domain, DID: the diaphanous inhibitory domain, DD: the dimerization domain, CC: a coiled-coil region, FH1: formin homology 1 domain, FH2: formin homology 2 domain, DAD: the diaphanous autoregulatory domain, FSI: formin–Spire interaction domain, PDZ: Postsynaptic density protein, Discs large, Zona occludens 1 domain, WH2: WASP homology 2 domain

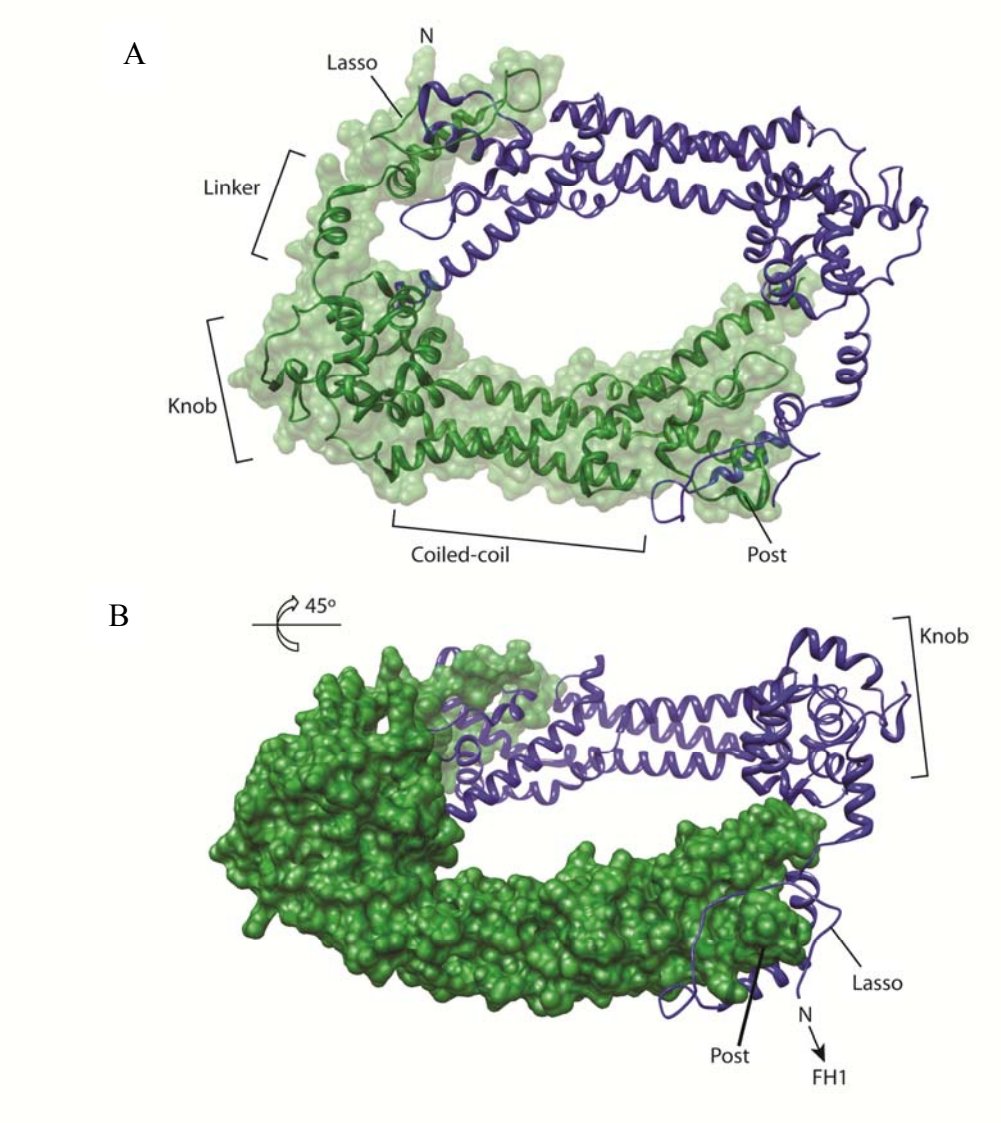

Figure 2. The FH2 Domain is a tethered dimer (adapted from Xu et al, 2004). (A) Three-Dimensional Structure of the FH2 domain. The diagram shows the overall architecture of the FH2 dimer. One monomer is in green, the other half is in blue. Each monomer possesses the lasso, linker, knob, coiled-coil, and post subdomains from the N to the C terminus. The halves interact through lasso-post interaction. The linker subdomains provide some flexibility to the dimer. (B) Side view of the FH2 domain dimer after rotating 45^{o}. The interactions between the post of one subunit and lasso of the other subunit are highlighted.

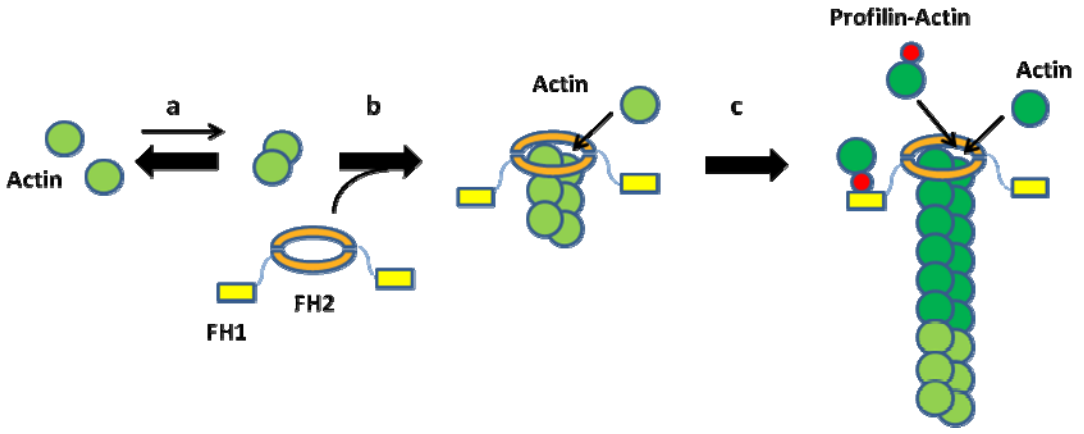

Figure 3 FH1FH2 dimer of processive formins nucleate actin filaments and stay at the filament barbed end as it elongates (adapted from Kovar, 2006). Spontaneous Nucleation is thermodynamically unfavorable. Dimers easily fall apart. FH1FH2 dimer stabilizes actin dimmers and promotes actin nucleation. Filament elongates while FH1FH2 dimer remain associated with the filament barbed end. Actin and profilin-actin can be added to the filament barbed end. Profilin-actin interacts with FH1 domains.

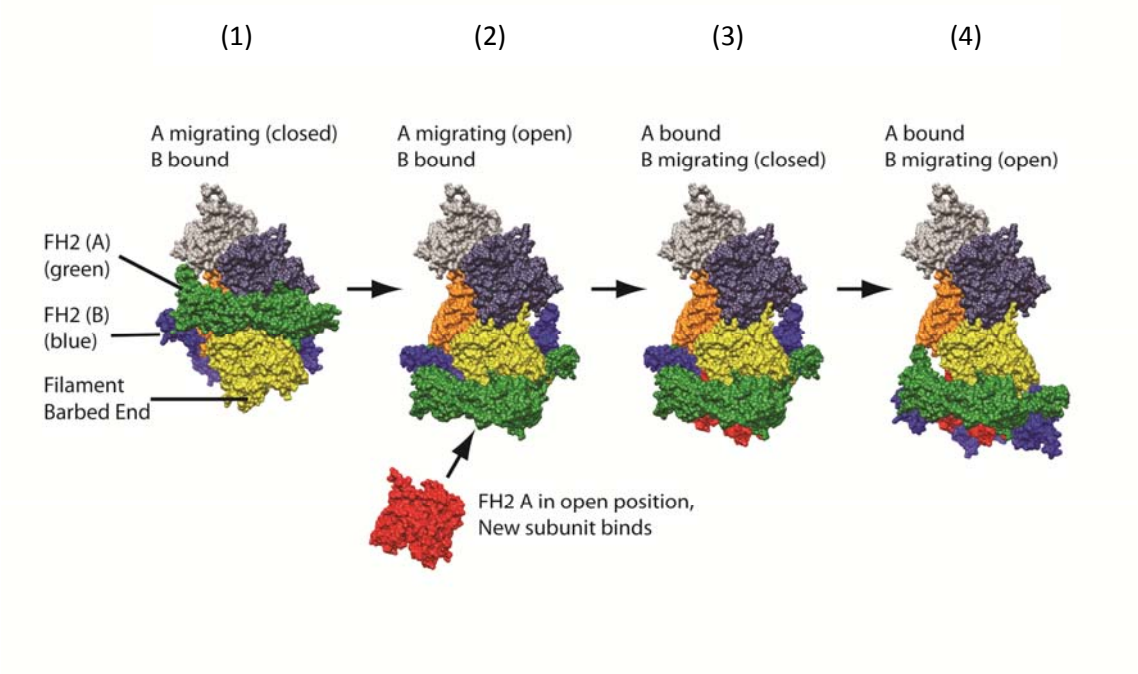

Figure 4 FH2 dimer moves processively at filament barbed end through the cooperation of the two FH2 monomers and actin subunits (adapted from Goode and Eck, 2007). The two FH2 monomers are colored in green (A) and blue (B). They work as two bridges by associating and dissociating with actin subunits at filament barbed end. In each round of actin subunit addition (step (1) to step (2)), one bridge (B) remains bound to two actin subunits tightly while the other bridge (A) is migrating. The migrating bridge (A) is moving from an upper position to a lower position. At the upper position, it interacts with two actin subunits and no place is available for subunit addition. Thus the bridge is in a closed state. The migrating bridge associates with only one actin subunit after migrating to the lower position. Its post subdomain is exposed for a new subunit. Thus actin addition is allowed. Actin addition is repeated in steps (3) and (4). However FH2 (B) is migrating now when FH2 (A) remains bound to the filament.

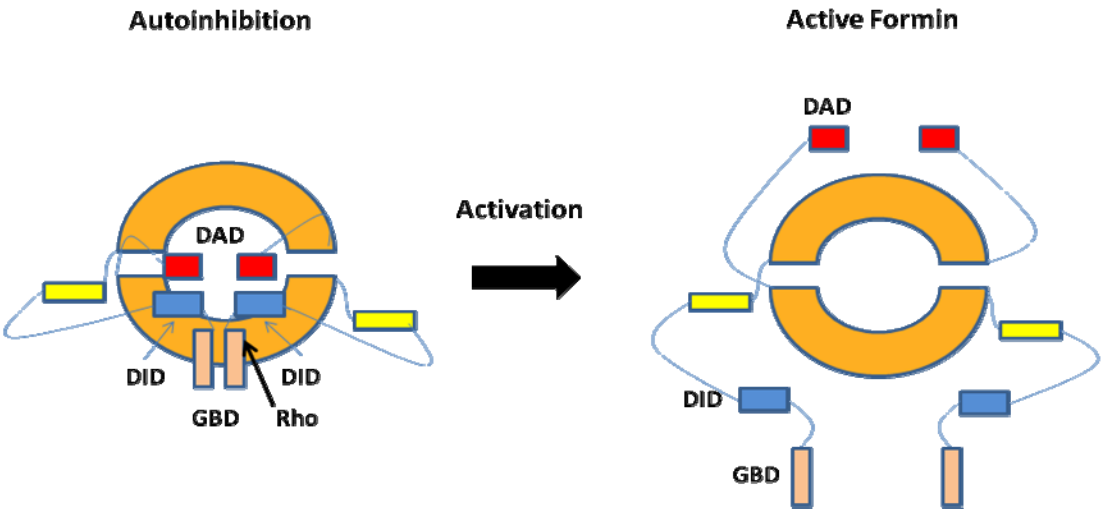

Figure 5. Diaphanous-related formins are regulated by autoinhibition. In the left panel, formin FH2 dimer is in an autoinhibited state due to the interaction between DID and DAD. The interaction between DID and DAD is disrupted by the binding of Rho GTPases to GBD. The resulting formin dimer is active (right panel). (adapted from Campellone, 2010).

Chapter 2

Research Plan

Background

Inverted Formins

The vertebrate inverted formin, INF2, is one of the most unusual formins characterized to date. The FH1 and FH2 domain of INF2 have the same effects on actin polymerization as most other formins but INF2-(FH1-FH2) is also highly potent in promoting actin filament assembly (Chhabra and Higgs, 2006). The assembly activity is similar to those of mDia1 and mDia2 and more than 100-fold higher than that of FRL1 (Harris et al., 2004; Harris et al., 2006). The rate of INF2-(FH1-FH2) mediated filament elongation is only 10% of free barbed end elongation rate (Chhabra and Higgs, 2006). Profilin increased barbed end elongation 20-fold in the presence of INF2 (Chhabra and Higgs, 2006). INF2 also contains a WASP Homology 2 motif C-terminal to FH2 domain, which has the ability to sequester actin monomers (Chhabra and Higgs, 2006). INF2 bundles actin filaments and can also sever and depolymerize filaments shortly after their formation (Chhabra and Higgs, 2006). Phosphate inhibits the depolymerization ability of INF2, suggesting that ATP hydrolysis on actin is a trigger for depolymerization (Chhabra and Higgs, 2006). An N-terminal DID has been identified by sequence analysis, and a putative DAD domain is found in C-terminus overlapping with the WH2 motif (Chhabra and Higgs, 2006). However, the DID-DAD interaction does not inhibit INF2 actin nucleation activity, indicating that INF2 is regulated by a different mechanism (Chhabra, 2009).

Although the N- and C-terminal interaction does not inhibit nucleation activity, it inhibits deploymerization activity (Chhabra, 2009). In cells, endogenous INF2 is bound to endoplasmic reticulum (ER) and is the first formin associated with ER function (Chhabra, 2009).

Although the vertebrate inverted formin INF1 is closely related to INF2, it has neither DID nor DAD domains. The C-terminal half of INF1 is composed of a unique amino acid sequence similar to a microtubule binding domain or MTBD (Young et al., 2008). INF1 links microtubules *via* MTBD domain to actin filaments. INF1 expressed in fibroblast cells induced actin stress fiber formation, co-alignment of microtubules with actin filaments, and the formation of acetylated microtubules (Young et al., 2008). Endogenous INF1 is associated with acetylated microtubules (Young et al., 2008). These findings indicated that INF1 is a microtubule-associated inverted formin and may have a role in regulating structures where microtubule organization plays an essential role.

Considering the common characteristics of formin members and the unique features of inverted formins, we hypothesize that (1) INFT-1 FH2 should be able to nucleate actin assembly. (2) INFT-1 FH1FH2 mediated barbed-end elongation rate would be increased by the addition of profilin. (3) INFT-1 FH1FH2 dimer can move processively at filament barbed end.

Formins in C. elegans

There are six formin genes present in *C. elegans* (see table 1), including INFT-1,

CYK-1 and FHOD1. In dividing eggs, CYK-1 protein is detectable only well after the initiation of furrow ingression, when it forms a ring at the leading edge of the cleavage furrow. CYK-1 was detected at the leading edge of the first cleavage furrow in five wild-type embryos when the contractile rings were 18 to 49% of the cell diameter (Swan et al., 1998) and plays a role in cytokinesis in the nematode worm early embryo (Neidt et al., 2008). CYK-1 mediated actin nucleation is inefficient comparing to Cdc12p, the formin required for cytokinesis in fission yeast (Neidt et al., 2008). However, CYK-1 is more efficient in promoting profilin-actin elongation than Cdc12p (Neidt et al., 2008). CYK-1 mediated actin assembly is inhibited by capping protein (Neidt et al., 2008).

Table 1: Six *C. elegans* formins (Higgs and Peterson, 2005; http://www. Wormbase.org, release WS223, date Feb 26 2011)

Group	Name	WormBase	Protein	Length(aa)	Notes
DAAM	daam-1	F56E10.2	WP:CE32443	813	excretory cells
FRL	frl-1	Y48G9A.4	WP:CE32979	1115	*Unknown function*
Dia	cyk-1	F11H8.4	WP:CE36535	1435	Splice A, embryo cleavage
			WP:CE36536	1437	Splice B, embryo cleavage
FHOD	fhod-1	C46H11.11	WP:CE41309	1346	vulva, pharynx, intestine
INF	inft-1	F58B6.2	WP:CE19472	881	distal tip, vulva, neuron system
INF	inft-2	F15B9.4	WP:CE37351	1140	*Unknown function*

INFT-1 – an Inverted Formin Potentially Involved in Cell Motility

INFT-1 is one of the six formin family members found in *Caenorhabditis elegans*. It belongs to INF (inverted formin) group, which are unique in the placement of their

FH1 FH2 domains at the N-rather than C-terminus, while all other formins contain additional domains N-terminal to the FH1. Nematode INFT-1 is most closely related to vertebrate INF2, an inverted formin with regulatory domains in the C- rather than N-terminus. We found by sequence alignment that nematode INFT-1 contains both formin homology 1 and 2 domains. However, it does not share the N-terminal diaphanous inhibitory domain (Hunt-Newbury et al.) and mid-sequence diaphanous autoregulatory domain found in vertebrate INF2 (Chhabra and Higgs, 2006). In contrast to INF2, nematode INFT-1 sequence starts immediately at a small putative dimerization domain (DD) followed immediately by the FH1 domain, and its C-terminal region shares little homology with INF2, suggesting that *C. elegans* INFT-1 might be regulated by other mechanisms.

During cell migration, formins promote the formation of actin networks to remodel cell architecture (Goode and Eck, 2007). A large scale expression study in *C. elegans* showed that INFT-1 is expressed in the larval pharynx, distal tip cell, developing vulva, and tail neurons (Hunt-Newbury et al., 2007). Intriguingly, its late-larval stage vulval expression pattern appears to overlap with descendents of the sex myoblast (SM) cell. As SM cells, distal tip cells, and developing neurons migrate, expression of INFT-1 in these cells suggests a role in cell migration.

Although the inverted formins, INF1 and INF2, from vertebrates have been partially characterized biochemically, few of these inverted formins have been studied to date. We do not yet know if their regulatory mechanisms or their C-terminal functions are conserved across other metazoan INFs. Furthermore, their role in cell

motility has not yet been elucidated. I have therefore purified and biochemically characterized the FH1 and FH2 domains of the inverted formin INFT-1 from C. elegans. Comparison to other INF family members will lend useful insight into the mechanisms of this unique class of formins.

Material and Methods

Plasmid constructs:

Bacterial expression constructs for full length INFT-1, INFT-1 FH1FH2, and INFT-1 C-terminus were prepared by the following cloning procedures: full length INFT-1, was amplified from *C. elegans* INFT-1 cDNA by polymerase chain reaction (PCR) using a pair of primers with two restriction sites, Nco I and HIND III. The primer sequences and the restriction sites they carry are shown as below:

Forward primer: CGAT(CCATGG)CGACGAGCGACACAATTCG

Reverse primer: CGCGCG(AAGCTT)TTACACCCATTTCGGTTTAGC

Nco I: 5'…. CCATGG…. 3'

3'…. GGTACC….5'

HIND III: 5'…. AAGCTT …. 3'

3'…. TTCGAA …. 5'

INFT-1 FH1FH2 and C-terminus were amplified from the PCR products of full length INFT-1. Primers for INFT-1 FH1FH2:

Forward primer: CGAT(CCATGG)CGACGAGCGACACAATTCG

Reverse primer:

CGCGCG(AAGCTT)TTACTTCTTCTCTTCTTTTTTCAATTTTCT-AG

Primers for INFT-1 C-terminus:

Forward primer: CGAT(CCATGG)AGACGCAGACGACGAGAG

Reverse primer:

CGCGCG(AAGCTT)TTACTTCTTCTCTTCTTTTTTCAATTTTCT-AG

Each DNA fragment was ligated into a TOPO blunt vector. Full length INFT-1, INFT-1 FH1FH2 and C-terminus were digested with restriction enzymes, Nco I and HIND III (Promega, Madison, WI). Each digested fragment was ligated to a pGV67 vector, which has an N-terminal GST tag. The vectors were sent for sequencing to confirm the identity of the inserts. The pGV67 system was not working well for INFT-1 FH1FH2 expression and purification. New PCR products were amplified from the pGV67 vector carrying full INFT-1. Four primers were designed with restriction sites Sal I and Xho I. The primer sequences and the restriction sites (in brackets) they carry are shown as below:

Sal I: 5'…. GTCGAC…. 3'

3'…. CAGCTG….5'

Xho I: 5'…. CTCGAG …. 3'

3'…. GAGCTC …. 5'

Primers for full length INFT-1:

Forward primer: CCGC(GTCGAC)TGACGAGCGACACAATTCGAC

Reverse primer: CGAC(CTCGAG)CACCCATTTCGGTTTAGCAGG

Primers for INFT-1 FH1FH2:

Forward primer: CCGC(GTCGAC)TGACGAGCGACACAATTCGAC

Reverse primer:

CGAC(CTCGAG)CTTCTTCTCTTCTTTTTTCAATTTTCTAGTCT-CC

Primers for INFT-1 C-terminus:

Forward primer: CCGC(GTCGAC)TGGAGACGCAGACGACGAGAG

Reverse primer: CGAC(CTCGAG)CACCCATTTCGGTTTAGCAGG

Each fragment was ligated into a TOPO blunt vector and digested by Sal I and Xho I (Promega, Madison, WI). Each digested fragment was ligated to a modified pET21a-MBP (TEV)-6HIS vector (a gift from Dr. David Kovar from University of Chicago) containing an N-terminal maltose binding protein (MBP) and Tobacco Etch Virus (TEV) cleavage site and a C-terminal 6x histidine tag. The constructs were sequenced to confirm the identity of each insert. Sequence verified pET21 vectors carrying full length INFT-1, INFT-1 FH1FH2, and INFT-1 C-terminus were transformed to bacteria strain BL21 DE3 for expression, respectively. A plasmid construct with nematode profilin isoform 1 was a gift from Dr. David Kovar.

Actin purification and modification

All protein purification procedures are carried out at 0-4 °C unless specified otherwise. Unlabeled Ca-ATP actin was purified from acetone powder of rabbit skeletal muscle (Kuhn, 2005). Actin monomers were polymerized and pelleted. The pellet was resuspended in buffer G (2 mM Tris-HCl, pH 8.0, 0.2 mM ATP, 1 mM NaN3, 0.1 mM $CaCl_2$, 0.5 mM dithiothreitol, DTT) , sonicated in a bath sonicator for 1 min or longer to speed up depolymerization. After sonication, resuspended actin

was diluted to 6 mg/ml and dialyzed against three – four changes of buffer G over 2 days to depolymerize the actin. After centrifugation at $1.1x10^5$ g for 2h, the top 80% of the supernatant of the crude actin was gel filtered on Sephacryl S-300 (Sigma, St. Louis, MO) to separate monomers from oligomers and minor contaminants. We determined the concentration of unlabeled actin by absorbance. The extinction coefficient is E_{290} = 26,600 $M^{-1}cm^{-1}$ (Kuhn, 2005). Labeled actin was prepared from crude monomeric actin from unlabeled actin preparation.

Pyrenelabeled actin purification (Pollard, 1984): Crude monomeric actin was dialyzed against two changes of dialysis buffer (10 mM TRIS-HCl, pH 7,5, 0.2 mM ATP, 0.1 mM $MgCl_2$, 1 mM sodium Azide (NaN_3)) for 1 h each. Actin was polymerized by adding an equal volume of 2X cold polymerization buffer (2X = 20 mM TRIS-HCl, pH 7.5, 0.2 M KCl, 0.4 mM ATP, 0.2 mM $MgCl_2$, 2 mM Azide (NaN_3)). After polymerizing for 5 min, actin was diluted to 1 mg/ml with cold polymerization buffer. A 10-mM stock solution of pyrene iodoacetamide (Molecular Probes, Eugene, OR) was prepared in N,N-dimethylformamide and stored at -20 °C. A 7-fold molar excess of pyrene iodoacetamide was added to the actin drop by drop while stirring gently. The solution was stirred gently overnight while protected against light. After labeling, actin was clarified at 3273X g for 10 min and centrifuged at $1.1x10^5$ g for 2 h to pellet actin filaments. The pelleted filaments were resuspended in buffer G, sonicated for 1 min, diluted to 6 mg/ml, and dialyzed for 1.5 – 2 days against two changes of buffer G to depolymerize actin. Pyrene labeled actin monomers were separated from oligomers by centrifugation at $1.1x10^5$ g for 2 h and

gel filtration on a Sephacryl S-300 (Sigma, St. Louis, MO). Fractions were stored at 4 °C protected against light. Labeled actin remained active for up to 2 months. The concentration of pyrene labeled actin was determined by measuring the absorbance at 290 and 344nm. The extinction coefficient of pyrene at 344nm E_{344} = 21,978 $M^{-1}cm^{-1}$ and a correction for pyrene absorbance at 290 nm of $A^{*}_{290} = A_{290} - 0.127A_{344}$.

Oregon Green labeled actin: Crude monomeric actin was dialyzed against two changes of buffer G without DTT for 1 h each. Actin was polymerized by adding an equal volume of 2X cold label buffer (2X = 50 mM imidazole, pH 7.5, 0.2 M KCl, 4 mM MgCl2, 6 mM NaN_3, 0.6 mM ATP). After polymerizing for 5 min, actin was diluted to 1 mg/ml with cold label buffer. A fresh 10-mM stock solution of Oregon Green (Invitrogen, Carlsbad, CA) was prepared in N,N-dimethylformamide and a 12-fold molar excess of Oregon green was added to the actin drop by drop while stirring gentlely. The solution was stirred gently overnight while protected against light. After labeling, actin was centrifuged at $1.1x10^5$ g for 2 h to pellet actin filaments. The pelleted filaments were resuspended in buffer G, sonicated for 1 min, diluted to 6 mg/ml, and dialyzed for 1.5 days against two changes of buffer G and one change of buffer G6.5 (5 mM PIPES-Tris, pH 6.5, 0.2mMATP, 1mMNaN_3, 0.1mM$CaCl_2$, 0.5mM DTT). Labeled actin was centrifuged at $1.1x10^5$ g for 2 h and top 80 – 90% supernatant was loaded onto a column of DEAE-cellulose DE52 (Whatman, Kent, UK), whick was equilibrated with buffer G6.5. Proteins were eluted with a gradient of 0.1 – 0.3 M KCl in buffer G6.5 (200ml each). Fractions from the peak to the highest salt were combined and dialyzed against buffer G. Dialyzed protein was concentrated

using Centricon centrifugal concentrators (10,000 MWCO, Amicon Ultra, Billerica, MA) at 3273X g to ~ 2 mg/ml. Concentrated proteins were dialyzed against 3 changes of buffer G in 1.5 days and centrifuged at $1.1x10^5$ g for 2 h. Top 80 – 90% supernatant was gel filtered on a Sephacryl S-300 (Sigma, St. Louis, MO). Fractions were stored at 0 – 4 °C protected against light. Labeled actin remained active for up to 4 weeks. The concentration of Oregon green labeled actin was determined by measuring the absorbance at 290 and 491nm. The extinction coefficient of Oregon green at 491nm E_{491} = 77,800 $M^{-1}cm^{-1}$ and a correction for Oregon green absorbance at 290 nm of $A^*_{290} = A_{290} - 0.16991A_{491}$.

Expression and Purification of Profilins and INFT-1

Profilins purification: CePFN-1 was purified from *E. coli* BL21 DE3 strain. Cell pellet was resuspended in buffer A (20 mM Tris-HCl pH 8.1, 1 mM EDTA, and 5 mM dithiotreitol), lysed using a digital sonifier (Branson, Danbury, CT) for 2.5 minutes and centrifuged at $8x10^4$ g for 30 minutes (Polet, 2006). The cleared supernatant was loaded to a poly-proline sepharose column. The column was washed with buffer A and protein was eluted with 6 M urea in buffer A (Polet, 2006). Ce PFN-1 concentration was determined by measuring the absorbance at 280 nm and by using the extinction coefficient 18, 450 $M^{-1}cm^{-1}$ (Polet, 2006).

Human profilin was purified as described in Almo et al, (Almo, 1994). Human profilin was purified from *E. coli* BL21 DE3 strain. Pelleted bacteria was resuspended in buffer I (20 mM Tris-HCl, pH 7.5,150 mM KCl, 0.2 mM DTT) and sonicated in a

digital sonifier (Branson, Danbury, CT) for 2 minutes and 30 seconds and centrifuged at 36355x g for 20 minutes. The cleared supernatant was loaded on a poly-proline sepharose column. The column was washed in buffer I and buffer I with 2 M urea. Protein was eluted with 7 M urea in buffer I. The fractions containing human profilin were pooled together and dialyzed against two changes of buffer I. Dialyzed protein was concentrated using Centricon centrifugal concentrators (3,000 MWCO, Amicon Ultra, Billerica, MA). Concentrated profilin was dialyzed against buffer I. Profilin was divided in small aliquots, flash frozen by liquid nitrogen and stored at -80 °C. The concentration of human profilin was determined by using an extinction coefficient 15,000 $M^{-1}cm^{-1}$ (Almo, 1994).

INFT-1purification: *Escherichia coli* strain BL21 DE3 transformed with pET21a-MBP (TEV)-INFT-1 FH1FH2-6HIS plasmid was grown in terrific broth (12g/L tryptone, 24g/L Yeast extract, 12.5g/L K_2HPO_4, 2.3g/L KH_2PO_4) at 37 °C until A_{600} reached 0.8. After the temperature was reduced to 25 °C, the culture was induced with 0.5 mM isopropyl β-D-thiogalactopyranoside for 6 hours at 25 °C and the *E. coli* cells were then collected at 4 °C. The following purification steps are carried out at 4 °C. The pelleted cells were resuspended in extraction buffer (50 mM NaH_2PO_4, pH 8, 500 mM NaCl, 10% glycerol, 10 mM BME) plus one tablet/50 ml of protease inhibitors, and sonicated on ice for a total of 2 minutes and 30 seconds in a digital sonifier (Branson, Danbury, CT). After 30 min centrifugation at 20,000 rpm, the homogenate was incubated with Talon (Clontech, Mountain View, CA) metal affinity resins for 40 minutes. The incubated sample with resins was loaded to a

disposable column. The resins were washed with 5 column volume of wash buffer (10 mM Imidazole, pH 7, 150 mM NaCl, 5 mM BME) plus 0.1% Thesit followed with 5 column volume wash buffer without Thesit. MBP (INFT-1 FH1FH2) 6X His was eluted with 50 ml of 100 mM Imidazole, pH 7 in wash buffer and dialyzed against cleavage buffer (50 mM Tris, pH 8, 100 mM NaCl, 0.5 mM EDTA, 1 mM DTT, 1 mM NaN_3) overnight. MBP (INFT-1 FH1FH2) 6X His was concentrated after dialysis using Centricon centrifugal concentrators (30,000 MWCO, Amicon Ultra, Billerica, MA). Concentrated INFT-1 FH1FH2 was cleaved with 10U/µl ProTEV protease (Promega, Madison, WI) to remove the MBP tag overnight. The cleaved proteins were dialyzed against Source Q buffer (25 mM Tris-HCl, pH 8.6, 50 mM NaCl, 1 mM EDTA, 1 mM DTT, and 1 mM NaN_3) for 6 hours. Dialyzed proteins were loaded to a 1 ml Souce Q column and eluted with Source Q buffer containing a linear gradient of NaCl from 50 mM to 1 M. Collected fractions were dialyzed against Source S buffer (20 mM HEPES, pH 6.5, 75 mM NaCl, 1 mM EDTA, 2 mM DTT, 1 mM NaN_3) for 6 hours and loaded to a 1 ml Source S column. INFT-1 FH1FH2 6X His was eluted by Source S buffer with a linear gradient of NaCl from 75 mM to 1 M. Pure INFT-1 FH1FH2 was dialyzed against formin buffer (20 mM HEPES, pH 7.4, 200 mM KCl, 1 mM EDTA, 1 mM DTT, 1% NaN_3) overnight and then dialyzed against formin buffer with 50% glycerol for 6 hours. INFT-1 FH1FH2 6X His was flash frozen by liquid nitrogen and stored at -80 °C. INFT-1 FH1FH2 6X His was used for up to a month before activity was lost. INFT-1 FH1FH2 concentration is determined by using an extinction coefficient 26030 $M^{-1}cm^{-1}$. The extinction

coefficient for INFT-1 FH1FH2 was estimated from the amino acid sequence by the method of Gill and von Hippel (Gill, 1989).

Pyrene actin polymerization by fluorescence spectroscopy

Spontaneous actin assembly fluorescence of 20% pyrene actin, excitation at 364 nm and emission at 407 nm was measured in Spectra MAX Gemini XPS fluorescence plate reader. Before measurement, 3.75 μM monomeric actin mixture (20% pyrene labeled) was placed in a lower row of a 96 well haft area flat bottom plate (Corning, Corning, NY). INFT-1 FH1FH2 and Ce PFN-1, were placed in a upper row of the same plate with 100X anti-foam (100X: 0.05% Antifoam 204), 5X KMEI (50 mM Imidazole, pH 7, 250 mM KCl, 5 mM $MgCl_2$, 5 mM EGTA), and Mg G buffer (2 mM Tris pH 8, 0.5 mM DTT, 1 mM NaN_3, 0.2 mM ATP, 0.1 mM $MgCl_2$). The reaction was started by transferring 100 μl actin mixture from the lower row and mixing it with the contents in the upper row with a 12-channel pipetman (Gilson, Middleton, WI). The final concentration of the proteins was indicated in the figure legends.

Nucleation Efficiency Data Analysis

Actin filaments concentrations were calculated from the plateau of pyrene assembly curves using a monomer critical concentration of 0.17 μM for experiments without profilin and 0.12 μM for experiments with profilin. Concentration of ends were calculated from the slopes at half-maximal polymerization using the formula $[ends] = slope / (k_+[A_{free}] - k_-)$ with association and dissociation rate constants of

k_+=12.9 $\mu M^{-1}s^{-1}$ and k_-=2.2 s^{-1} respectively without profilin and k_+=11.6 $\mu M^{-1}s^{-1}$ and k_- =1.4 s^{-1} with profilin. Nucleation efficiency, or number of ends generated per formin dimer, was calculated from linear fits of the concentration of ends at half-maximal polymerization as a function of formin dimer concentration.

Total Internal Reflection Fluorescence (TIRF) Microscopy

Actin at a concentration of 1.5 µM (33% Oregon green labeled) was mixed with INFT-1 FH1FH2, Ce PFN-1, and 2X TIRF buffer (final 1X: 10 mM Imidazole pH 7, 50 mM KCl, 1 mM $MgCl_2$, 1 mM EGTA, 100 mM DTT, 0.2 mM ATP, 15 mM Glucose, 0.25% Methyl Cellulose (1500 centipoises), 20 µg/ml catalase, 0.1 mg/ml glucose oxidase) to start spontaneous actin assembly. Approximately 16 µl of the mixture was wicked through a flow-cell, which was coated with NEM-Myosin and blocked by BSA (Kuhn, 2005). The Oregon green labeled filaments were excited by total internal reflection (from Olympus BX51WI) and the images were collected by a QImaging ROLERA-MGi camera at a 10 s interval.

Filament growth rate measurement

The images taken from TIRF microscopy were analyzed in ImageJ. The length of each filament was measured frame by frame (Kuhn, 2005). The length was plotted against time in Excel and the growth rate was calculated for each filament.

Statistics Analysis

We used unpaired student T-test to analyze the results of at least 3 filaments per experiment and three experiments for each condition. The control group and treated group are independent of each other. The variance of each group is unknown. Thus T-test is good choice under the assumption that data from the same group have equal variances.

Results

Cloning of C. elegans INFT-1

We used a *C. elegans* cDNA library to construct expression vectors for full length INFT-1, for the N-terminal FH1-FH2 domain, and for the putative C-terminal regulator domain of INFT-1. PCR was used to amplify the full length INFT-1 from *C. elegans* cDNA using primers containing Sal I and Xho I restriction sites at the N terminus and C terminus, respectively. The N-terminal FH1-FH2 domain and for the potential C-terminal regulator domain of INFT-1 are amplified from the full length fragment. Agarose electrophoresis of the amplified products showed bands of the expected size of 2,529 bp for full length, 1,521 bp for INFT-1 FH1FH2, and 1,008 bp for INFT-1 C-terminus (Figure 6). The three DNA fragments were placed into a modified pET21a expression vector and PCR was used to confirm the existence of the inserts in the vector (Figure 7) containing an N-terminal Maltose Binding Protein (MBP) tag followed by a tobacco etch virus (TEV) cleavage site and a C-terminal 6-Histidine tag. In earlier, GST tagged fusions of INFT-1, we found that expressed protein readily aggregated into inclusion bodies. Addition of an N-terminal MBP tag stabilized INFT-1 and increased its solubility upon expression. Each fragment was inserted between the two restriction sites: Sal I and Xho I within the multiple cloning region in pET21a vector and all three were verified by sequencing. The map of the vector carrying full length INFT-1 and the whole sequence is shown in Figure 8. Plasmids carrying full length INFT-1, INFT-1 FH1FH2, and INFT-1 C-terminus were

transformed to *E. coli* strain TOP 10 for plasmid replication and strain BL21 DE3 for protein expression, and strains were stored at -80 °C.

Purification of C. elegans inverted formin INFT-1 FH1FH2 domain

E. coli containing the modified pET21a vector with MBP-TEV-(INFT-1 FH1FH2)-6His was cultured at 37 °C in terrific broth and induced at 25 °C. Samples of crude lysates from the cultures induced at 25 °C were taken at 1, 2, 4, 6, and 16 hours. All samples showed the induction of the fusion protein MBP-TEV-(INFT-1 FH1FH2)-6His at the predicted molecular weight, 98 kDa, with maximum expression at 6 hours (Figure 9A, lane 3). *E. coli* were cultured in either Luria broth or terrific broth and induced at either 37 °C or 25 °C. Terrific broth gave significantly more protein expression than Luria broth, with maximal expression 6 hours after induction at 25 °C. We pelleted one liter of bacteria induced with these optimal conditions for subsequent INFT-1 FH1FH2 purification. The harvested bacteria cells were stored at -20 °C for about a week before use.

MBP-TEV-(INFT-1 FH1FH2)-6His was affinity purified on a Talon metal affinity column that binds specifically to the 6-Histidine tag. Bacteria pellets were homogenized in extraction buffer (50 mM NaH_2PO_4, pH 8, 500 mM NaCl, 10% glycerol, 10 mM BME) with 2.5 minutes of sonication. Cell debris was pelleted at 20,000 rpm for 30 minutes and supernatant containing crude cell lysate was passed over the resins. The resin was washed twice, one in wash buffer (10 mM Imidazole, pH 7, 150 mM NaCl, 5 mM BME) plus 0.1% Thesit, and one in wash buffer alone.

Tagged protein was eluted with elution buffer (100 mM Imidazole, pH 7, 150 mM NaCl, 5 mM BME) and collected. SDS-PAGE Gel electrophoresis (Figure 9A) showed predominant band at the expected size of 98 kDa for MBP-TEV-(INFT-1 FH1FH2)-6His. I cleaved the MBP tag with TEV protease overnight at 4°C. MBP-TEV-(INFT-1 FH1FH2)-6His cleavage yielded three bands of the anticipated size of 98 kDa for MBP-TEV-(INFT-1 FH1FH2)-6His, 56 kDa for (INFT-1 FH1FH2)-6His, and 42 kDa for MBP tag (Figure 9B). We separated the FH1FH2 fragment from MBP and uncleaved protein on a mono Q anion exchange column in mono Q buffer (25 mM Tris-HCl, pH 8.6, 50 mM NaCl, 1 mM EDTA, 1 mM DTT, 1 mM NaN_3) eluted by a gradient of NaCl from 50 mM to 1M in mono Q buffer. Fractions containing both (INFT-1 FH1FH2)-6His and MBP tag were applied to a mono S cation exchange column to separate (INFT-1 FH1FH2)-6His from cleaved MBP. FH1FH2 was eluted in mono S buffer (20 mM HEPES, pH 6.5, 75 mM NaCl, 1 mM EDTA, 2 mM DTT, 1 mM NaN_3) in a 75 mM – 1M gradient of NaCl. Gel electrophoresis showed a near-homogeneous band at 56 kDa (Figure 9C). We dialyzed fractions with pure (INFT-1 FH1FH2)-6His in formin buffer (20 mM HEPES, pH 7.4, 200 mM KCl, 1 mM EDTA, 1 mM DTT, 1% NaN_3), concentrated protein by centrifugation using centrifugal concentrators (30, 000Amicon Ultra, Billerica, MA), flash froze aliquots in liquid N_2, and stored in formin buffer at -80 °C for up to one month. Aliquots stored longer than 1 month showed decreased activity.

C. elegans inverted formin INFT-1 assembles actin filaments

We tested the effects of INFT-1 FH1FH2 domain on the assembly of pyrene labled rabbit muscle skeletal actin (RMSA) using fluorescence spectroscopy (Figure 10). Pyrene labeled actin monomers have a low fluorescence signal that increases by 20-fold upon assembly. Increase in fluorescent emission over time after addition of KCl (to initiate reaction) is shown in Figure 10, where the slope of each line represents the rate of polymer assembly and is proportional to both the polymerization rate and the number concentration of free filament ends. INFT-1 FH1FH2 promotes the assembly of Mg-ATP actin monomers into filamentous actin. In the control, actin-alone reaction, a lag at the beginning of the reaction indicates inefficient nucleation (few ends). INFT-1 FH1FH2 reduces the lag time and thus promotes actin nucleation. INFT-1 FH1FH2 also enhances the assembly rate (Figure 10A), which could be due either to an increase in the concentration of ends or acceleration of the monomer association rates. The FH1FH2 accelerates polymerization in a concentration dependent manner.

Total Internal Reflection Fluorescence (TIRF) microscopy provides additional evidence that worm INFT-1 FH1FH2 enhances actin assembly by promoting actin nucleation. In TIRF experiments, we use Mg-ATP actin labeled with Oregon green 488 to observe the dynamic formation of single actin filaments. Moderate photobleaching of Oregon green 488 allows us to differentiate the slow-growing pointed end and fast- growing barbed end. The subunits near the barbed end are always brighter than those near the pointed end. Actin assembly in the absence or

presence of INFT-1 FH1FH2 reveals difference in filament number and length. Actin nucleation is more efficient in the presence of INFT-1 FH1FH2 (Figure 11 C). In the same area of an observing field and over the same amount of time, there were many more actin filaments nucleated by INFT-1 FH1FH2 than those nucleated *de novo* (Figure 11 A, C). Filaments nucleated in the presence of INFT-1 FH1FH2 are shorter comparing to the ones nucleated in the absence of INFT-1 FH1FH2. Since the amount of actin monomers is the same in both reactions, shorter filaments also indicate that INFT-1 FH1FH2 enhances nucleation.

INFT-1 slightly reduces the actin barbed end elongation rate

Actin assembly involves two stages, nucleation and elongation. Although INFT-1 enhances overall actin assembly rate and promotes nucleation, increased polymerization rates seen in pyrene-actin assembly assays could be in part due to increased monomer association rates rather than entirely due to nucleation.

TIRF microscopy provides accurate quantification of the filaments barbed end elongation rates. Microscopy allows us to measure the lengths of individual elongating filaments at both ends. In time-lapse TIRF movies, we traced single filament assembly and measure the length growth at each end to calculate the growth rate. A mixture of 1.0 μM Mg-ATP actin plus 0.5 μM Mg-ATP actin monomers labeled with Oregon Green was flowed through the chamber in the absence or presence of INFT-1 FH1FH2. The slides were coated with inactive NEM myosin-II (rigor myosin) before each reaction that randomly captures actin filaments. Points of

myosin capture appeared as rigid constriction points amidst thermal fluctuations in filament position and orientation in maximum intensity projections of filament life histories. Myosin constriction points were used as a permanent fiduciary mark along the filament to separate length measurements into barbed end and pointed end halves. Length changes of individual filaments are shown as kymographs over time in Figure 11 B and D, with the fast growing end as the barbed end. INFT-1 FH1FH2 slightly reduces the actin filament barbed end growth rate (Figure 11D) in comparison to the rate of free barbed end growth (Figure 11 B). Control filaments elongated at the barbed end at a rate of 16.4 ± 0.9 subunits/s (n = 20) (Figure 12 A) in the absence of INFT-1 FH1FH2 and the rate decreased to 15.7 ± 1.1 subunits/s (n = 12) if INFT-1 FH1FH2 is present (Figure 12 B). This decrease (P = 0.0324) indicates that INFT-1 slightly affects filament barbed end elongation.

The actin assembly rate mediated by INFT-1 decreased in the presence of profilin

Profilin is an actin monomer binding protein that inhibits spontaneous actin assembly by hindering actin nucleation. Formins, on the other hand, enhance actin nucleation. Profilin interacts with the multiple poly-proline regions found in formin FH1 domains. Thus profilin and formin FH1 domain interact to affect actin polymerization. Since most formins processively attach to filament barbed ends, the interaction between profilin and poly-proline regions in formin FH1 domain will increase the local concentration of profilin-actin complex around the filament barbed end. Actin elongation rate mediated by processive formins will increase in the

presence of profilins. Formin constructs lacking profilin-binding FH1 domain still display a decrease in actin filament barbed-end elongation rate. FH1 domain is essential in interacting with profilin and increasing the local actin concentration near filament barbed end.

Both human profilin (Hs Pfn) and *C elegans* profilin 1 (Ce PFN-1) inhibit actin assembly (Figure 10C and E), while FH1FH2 promotes actin nucleation (Figure 11B) rather than elongation. In support of the lack of processivity of INFT-1, FH1FH2 mediated actin assembly rate is not increased by either Hs profilin or *C. elegans* profilins. The reaction has 2.5 μM Mg-ATP actin monomers (20% pyrene-labeled actin) and 2.5 μM Hs profilin or Ce PFN1 with different amount of INFT-1 FH1FH2. The reactions with lower concentration (5-20 nM) of INFT-1 FH1FH2 are similar in assembly comparing to the control reaction with actin only (Figure 10C and E). They are much slower than the reactions with the same amount of INFT-1 FH1FH2 but no profilins (Figure 10A, C, and E). It takes 20 nM INFT-1 FH1FH2 for Hs profilin, and 30 nM for Ce PFN1 to "recover" the actin assembly to control level with actin only. These results indicate that the interaction between INFT-1 and profilins does not increase the barbed end elongation rate.

Pyrene-actin assays cannot uniquely distinguish between nucleation and elongation, so we used TIRF microscopy to trace elongation of individual filaments. We flowed 1.5 μM Mg-ATP actin monomers (1/3 Oregon Green labeled actin) and/or 3 μM Ce PFN1 to NEM Myosin-II coated slides with 16 nM INFT-1 FH1FH2. Four images from each time lapse TIRF movie are shown in figure 11C, G with time

indicated on top left. Typical filament growth for each condition is displayed as straightened filament kymographs (length on y-axis and time on x-axis) (Figure 11 D, H). The slope of the fast increase end represents the barbed end growth rate and the slope of the slow increase end corresponds to the pointed end addition rate. When Ce PFN1 is present, barbed end growth (Figure 11H) is slightly slower than in the absence of profilin (Figure 11 D). The distribution of growth rates of several filaments are shown in Figure 12 in the absence and presence of both INFT-1 and Ce PFN-1. INFT-1 nucleated actin filament barbed ends elongate at 15.7 ± 1.1 subunits/s in the absence of Ce PFN-1, and 8.7 ± 1.1 subunits/s in the presence of Ce PFN1 (Figure 12B, D). INFT-1 mediated barbed end elongation rate decreased in the presence of Ce PFN-1. In contrast, most other formins investigated up to date show an increase in barbed end elongation rate upon the addition of profilin, making INFT-1 unique.

INFT-1 is a non-processive formin

We sought to determine whether INFT-1 could move processively along growing filament barbed ends. All formins characterized to date move processively along barbed ends with the exception of the non-processive *Arabidopsis* FORMIN1 (AFH1). Difference formins possess different efficiency in actin nucleation. The comparison between INFT-1 and other formins in nucleation efficiency may provide some hints about the characteristic regarding to the movement at filament barbed ends. The nucleation efficiency of INFT-1 FH1FH2 was determined by using the half maximum polymerization slope from the pyrene fluorescence assay curves in Figure 10A

(Michelot, 2005). The barbed ends concentration is shown in Figure 10B on y-axis, and the formin concentration is on x-axis. A linear fit shown by the line in Figure 10B depicts the relationship between these two concentrations. INFT-1 FH1FH2 generates 0.0183 ± 0.006 filament barbed ends per formin molecule at maximum. It was reported that *Arabidopsis* AFH1 can generate 0.026 filament barbed ends per molecule (Michelot, 2005). This INFT-1 FH1FH2 is slightly less efficient than *Arabidopsis* AFH1. It was also reported that *Arabidopsis* AFH1 is about 10 times more efficient than *Arabidopsis* AtFH5, as efficient as Bni1p, and 10 times less efficient than mDia1 and Cdc 12p (Michelot, 2005). In the presence of human profilin, INFT-1 FH1FH2 generates 0.00648 ± 0.00015 filament barbed ends per molecule at maximum. In the presence of Ce PFN1, the number is 0.00343 ± 0.00013. INFT-1 FH1FH2 efficiency decreased when we added human profilin or Ce PFN1 to the reaction. INFT-1 displayed a lower efficiency with Ce PFN1 than that with human profilin. However, we expected a higher efficiency with Ce PFN1 because INFT-1 is also from *C. elegans*.

Some of the difference between nematode and human profilin could be due to cross-species differences in affinity. Although both profilin and formin are from *C. elegans,* we used rabbit skeletal muscle actin rather than nematode actin. Rabbit skeletal muscle actin is a frequently used standard for assembly assays, and has allowed researchers to study the effects of formins from different species on a single type of actin. Nevertheless, we expect that C. elegans profilin and formin would likely have a higher affinity for C. elegans profilin than for rabbit actin.

The "stair-stepping" model explains how different formins slow down the elongation at filament barbed end. Formin FH2 domains form a flexible tethered dimer that binds to the filament barbed end (Xu et al, 2004; Otomo et al, 2005b). Each FH2 domain is in equilibrium between an open state that permits the addition of actin subunits to the barbed end and a closed state that inhibits the addition (Aditya and Pollard, 2009). Mouse mDia 1 reduces filament barbed end elongation rate by only ~10% and thus spends more time in the open state. Yeast Cdc12p severely reduces the rate of addition of actin subunits to the barbed end. Thus, Cdc12p preferentially maintains the closed state. For INFT-1, TIRF microscopy shows only a slight decrease of the barbed end elongation rate (Figure 11B and D, Figure 12A, B, and E). As a result, INFT-1 FH1FH2 dimer remains primarily in the open state. The preference for the open state indicates that INFT-1 likely attaches non-processively or with low processivity to filament barbed ends.

A hallmark of processive elongation is the ability of a tethered formin to remain attached to a growing barbed end. When formin is attached to the surface of a glass slide and filament elongation observed with TIRF microscopy (Kovar, 2006), processively attached barbed ends remain attached to a single point on the slide as they elongate. Filaments either spin around their barbed-end attachment points, or buckle if tethered along their side by rigor myosin attached to the slide surface. We used TIRF microscopy in an attempt to directly visualize processive actin assembly on tethered formin dimers. Similar to previous experiments (Kovar, 2006), we added Oregon green labeled actin to a glass slide coated with MBP-(INFT-1 FH1FH2).

Although surface-bound MBP-(INFT-1 FH1FH2) increased actin nucleation, filament barbed ends (yellow arrow, Figure 13A) moved freely as they grew, indicating that MBP-(INFT-1 FH1FH2) dimer is not processively associated with filament barbed end.

All processive formin members investigated to date show increased barbed end elongation rates in the presence of profilin, while profilin has no effect on the barbed end rate of non-processive formins (Michelot, 2006). We found that INFT-1 FH1FH2 slows down filament barbed end elongation slightly in the presence of Ce PFN1. The barbed end elongation rate of Ce PFN1-actin complex was 10.4 ± 1.1 subunits/s in the absence of INFT-1 FH1FH2 and 8.7 ± 1.1 subunits/s in the presence of INFT-1 FH1FH2 (p-value= 0.0075) (Figure 12C, D). This can be explained by the non-processivity feature of INFT-1 FH1FH2. Since INFT-1 FH1FH2 does not associate with the filament barbed end processively, the interaction between FH1 domain and Ce PFN1 will not affect filament barbed end elongation. Thus, the barbed end elongation rate is not increased by Ce PFN1. Ce PFN1 and INFT-1 FH1FH2 both slightly slow down actin filament barbed end elongation. The rate in the presence of both proteins is less than that in the presence of Ce PFN1 alone.

We also used glass slides coated with both MBP-(INFT-1 FH1FH2) and NEM-Myosin II to study the interaction between actin filament barbed and MBP-(INFT-1 FH1FH2). NEM-Myosin can randomly capture a point along a single actin filament. If the filaments are initiated by processive formins, such as mouse mDia1 and mDia2, filaments buckle as they grow because the new subunits are

always added between the formin dimer and actin filament barbed end. The segment between the NEM myosin attachment point and formin-barbed end attachment point elongates and buckles. Non-processive formins such as *Arabidopsis* FORMIN1 (AFH1) do not buckle filaments because they cannot capture elongating barbed ends (Michelot, 2006). We used TIRF microscopy to search for filament buckling between tethered MBP-(INFT-1 FH1FH2) and NEM-Myosin II. Filaments nucleated by tethered INFT-1 did not buckle. The movie shown in Figure 13C taken from the slide coated with MBP-(INFT-1 FH1FH2) and NEM-Myosin II is similar to the movie shown in Figure 11C taken from the slide coated with NEM-Myosin II alone. It is evident that INFT-1 FH1FH2 is not processively attached to actin filament barbed end. Annealing events (one filament's pointed end connects to another filament's barbed end) frequently occur even if MBP-(INFT-1 FH1FH2) is immobilized on the slide. Annealing events also indicate that MBP-(INFT-1 FH1FH2) is not settled on the filament barbed end (Figure 13B). All the evidences revealed the non-processivity of *C. elegans* INFT-1.

INFT-1 binds to filament sides and pointed ends.

Nonprocessive plant formins have been shown to bind to the sides of actin filaments (Michelot, 2006) rather than at barbed ends. To determine where on actin filaments INFT-1 binds, we coated 0.5 micron beads coated with 0.5 μM MBP-(INFT-1 FH1FH2) to use in TIRF microscopic assays of growing filaments. Labeled actin and pre-coated 0.5 micron beads were added together onto a glass slide

coated with 1% BSA. Filament nucleation was greatly enhanced at the surface of MBP-(INFT-1 FH1FH2) coated beads (Figure 14A) and filaments remained attached to the bead to form a radial "star" of dense polymerizing actin filaments centered on the bead. If formin remained processively attached to barbed ends, we would expect barbed ends to remain near the bead surface. If formins remain attached to the sides or pointed ends of newly nucleated filaments, barbed ends would radiate outward. To determine the orientation of INFT-1 bead nucleated filaments, we photobleached existing filaments with 10 seconds of continuous TIRF excitation. After photobleaching, filament tips that grew outside of the photobleached spot immediately increased in brightness (Figure 14D), indicating incorporation of newly labeled subunits. Thus, filament barbed ends were directed away from the bead. Fluorescence of the bleached spot gradually increased in brightness. Radial kymographs showed that the brightness for the photobleached spot increased from the center outward, indicating further nucleation of filaments at the bead surface. Thus, pointed ends remained near the MBP-(INFT-1 FH1FH2) coated beads and barbed ends grew away from the INFT-1.

Nucleotide state influences filament barbed end elongation rate

After Mg-ATP actin monomers polymerize into filamentous actin, actin subunits rapidly hydrolyze bound ATP to form Mg-ADP-Pi actin with a half time of 4 seconds, while the gamma phosphate is slowly released from actin subunits with a half-time of 6 minutes. Controlling the ATP vs. ADP-Pi state of actin subunits requires replacing

the bound ATP with a non-hydrolyzable ATP analog. In contrast, Pi release can be readily inhibited with excess phosphate in the polymerization buffer. To determine if formin influences the nucleotide state of actin subunits after polymerization, we explored the effects of excess phosphate on formin-mediated actin assembly with TIRF microscopy. Actin was polymerized as above in TIRF buffer containing 25 mM PO_4^{3-} but osmotically balanced with KCl to the same osmolarity as low phosphate TIRF buffer. We measured the growth of single filament pointed and barbed ends as above. Figure 15B shows kymographs of filament growth in high Pi buffer. When extra phosphate is present, the barbed end elongation rate (slope in Figure 15B) is slower than the rate without phosphate in Figure 11B. It indicates that phosphate might have some effects on actin assembly. We calculated the association rate of actin subunit at the pointed end and the barbed end. In 1.5 μM actin, the filament barbed end elongates at a rate of 16.4 ± 0.9 subunits/s (Figure 12 A) in the absence of phosphate and the rate decreases to 14.1 ± 1.1 subunits/s if extra phosphate is added to the system (Figure 16 A). The difference between the two rates are significant with a $P<0.0001$. When phosphate is present in the system, the elongation rate at filament barbed end is slightly slower than the rate when phosphate is absent in the system.

We tested whether phosphate influences INFT-1 mediated actin assembly by adding 16 nM INFT-1 FH1FH2 to the polymerization reaction in Fig 15C. We measured barbed end elongation rates from TIRF movies. Filament elongation kymographs (15D) showed an obvious slowing of INFT-1 mediated barbed end elongation in the presence of 25 mM excess phosphate. In excess phosphate buffers,

the native actin addition rate at the barbed end is 14.1 ± 1.1 subunits/s (Figure 16A) in the absence of INFT-1 FH1FH2, while the rate drops to 12.4 ± 1.3 subunits/s in the presence of INFT-1 FH1FH2 (Figure 16B). The difference between these two rates is significant with a $P = 0.003$ and it is similar to the difference between the rates in Figure 12A and B. We concluded that phosphate affects INFT-1 assembly activity on actin, but it is a small effect.

In *vivo*, polymerization-competent actin is found primarily as a profilin-actin complex. We therefore tested the effects of phosphate on profilin-actin polymerization by adding Ce PFN1 to high-phosphate TIRF actin polymerization reactions with or without INFT-1 FH1FH2. We measured profilin-actin polymerization in osmotically balanced buffer containing 25 mM excess phosphate. In the absence of INTF-1 (Fig. 15E), barbed elongation appeared slower in excess phosphate than in the absence of phosphate. We measured individual filament elongation rates as above and found that profilin-actin barbed end elongation dropped from 10.4 ± 1.1 subunits/s (Figure 12C) in the absence of phosphate to 8.5 ± 0.7 subunits/s in the presence of phosphate (Figure 16C). The difference ($P < 0.0001$) between these two rates indicates that phosphate slightly slows barbed end elongation when actin is bound to profilin (Ce PFN1). Therefore, phosphate does not have a strong effect on profilin-actin assembly.

In the presence of 16 nM INFT-1 FH1FH2, barbed end elongation of profilin-actin was slowed (Figure 15H). Addition of INFT-1 FH1FH2 dropped profilin-actin barbed end elongation from is 8.5 ± 0.7 subunits/s to 6.1 ± 0.5

subunits/s in high phosphate buffers (Figure 16C, D). The difference is significant with a $P < 0.0001$. The actin barbed end elongation rate in the presence of INFT-1 FH1FH2 was ~28% slower than the rate in the absence of INFT-1 FH1FH2 when phosphate is added to both reactions. This INFT-1 mediated decrease in barbed end elongation in high-phosphate buffers was much greater that the ~4% slowdown seen in the absence of excess phosphate (Figure 12C and D). Thus, phosphate enhances INFT-1 FH1FH2 mediated decrease in filament barbed end elongation when the actin monomers are bound to profilin (Ce PFN1).

Discussion

We studied the actin assembly features of an inverted formin from *C. elegans*, called INFT-1. We found that an INFT-1 construct containing active FH1FH2 domains nucleate actin filaments but had little impact on actin filament barbed end elongation. We also found features that are uncommon in formin family proteins. *C. elegans* INFT-1 does not increase actin filament barbed end addition rate in the presence of profilin, nor does it processively associate with the actin filament barbed end after nucleating filaments. We also found that the actin assembly activity of *C. elegans* INFT-1 is possibly influenced by the nucleotide state of polymerized actin subunits.

C. elegans INFT-1 has been demonstrated to assemble actin filaments by pyrene fluorescence spectroscopy assay and total internal reflection fluorescence microscopy. In pyrene fluorescence spectroscopy assays, INFT-1 FH1FH2 enhanced the total assembly rate as indicated by an increased polymerization slope (Figure 10) and reduced lag-time at the beginning of the reaction. The reduction in lag-time implies that INFT-1 FH1FH2 nucleates actin filaments. TIRF microscopy provided direct evidence that *C. elegans* INFT-1 FH1FH2 enhances the *de novo* nucleation rate (Figure 11). Thus, INFT-1 is an actin nucleator. The nucleation activity of *C. elegans* INFT-1 FH1FH2 does not depend on profilins because it nucleated more actin filaments in the absence of profilin (Figure 11A and C) than in the presence (Figure 11E and G). INFT-1 FH1FH2 nucleation efficiency is slightly less than the efficiency

of *Arabidopsis* AFH1 and Bni1p. INFT-1 is more efficient than *Arabidopsis* AtFH5, but less efficient than mouse mDia and yeast Cdc12p. INFT-1 nucleation efficiency decreased when human profilin or Ce PFN1 was present in the system. *C. elegans* INFT-1 FH1FH2 lowers the actin barbed end elongation rate by a small fraction regardless of profilin, although profilin also reduces the barbed end elongation rate slightly. Since *C. elegans* INFT-1 FH1FH2 increases the total actin assembly rate in pyrene fluorescence spectroscopy assay and TIRF microscopy showed that INFT-1 FH1FH2 enhances nucleation rather than elongation. Thus, INFT-1 FH1FH2 promotes actin polymerization by enhancing actin nucleation rather than by enhancing barbed end elongation rates. This is consistent with many other formin members such as mouse mDia1, mDia2, and yeast Cdc12p (Kovar, 2006) that decrease the actin filament barbed end elongation rate at different levels while enhancing actin nucleation.

C. elegans INFT-1 mediated actin filament barbed end elongation rates do not increase in the presence of profilins but rather decrease. In contrast, other formin members such as mouse mDia1 and mDia2 accelerate barbed end elongation in the presence of profilin (Kovar, 2006). Profilin increases the barbed end elongation rate ~5 fold for mDia1 and ~10 fold for mDia2 (Kovar, 2006). Two factors may contribute to this difference among different formins:

(1) Profilin increases the barbed end elongation rate of formin by interacting with the poly-proline regions in formin FH1 domain. In the reaction, profilin-actin complex binds to any of the several available poly-proline regions of FH1. Thus FH1

domain increases the local concentration of polymerization competent profilin-actin near the barbed end. The barbed end elongation rate, which is positively related to the substrate actin concentration, increases due to a relative increase in concentration. The mDia1 and mDia2 constructs used previously (Kovar, 2006) possess five or more poly-proline regions, while INFT-1 FH1FH2 construct only has three poly-proline regions. The interaction between INFT-1 FH1FH2 and profilins may not be as efficient as in mDia family formins due to the insufficient poly-proline regions at the profilin binding-site or a lower affinity of each for profilin binding. Thus INFT-1 likely does not increase the local concentration of actin near the filament barbed end to the extent of other formins. As a result, profilin would not affect the elongation rate as it does in other formins.

(2) *C. elegans* INFT-1 FH1FH2 does not move processively as the filament barbed end grows. The low affinity of INFT-1 FH1FH2 to filament barbed end implies that INFT-1 FH1FH2 dissociates from filament barbed end very fast. Even if the interaction between INFT-1 FH1FH2 and profilin is efficient, INFT-1 FH1FH2 cannot maintain a high local concentration of actin near the barbed end if it is not at the barbed end. The actin concentration at the barbed end for non-processive formins would be similar to the control reaction in the absence of formin. Since profilin also slightly inhibits actin filament growth, the elongation can be slower than the elongation without profilin. We note that 16 nM formin used in TIRF microscopy assays is at least 2-3 orders of magnitude greater than the concentration of free ends in the solution. Thus, the decrease in assembly rates seen in the presence of INFT-1

FH1FH2 domains is likely due to frequent, temporary binding of INFT-1 to barbed ends.

As show by multiple tests, we found that *C. elegans* INFT-1 is a non-processive formin. INFT-1 FH1FH2 binds to actin filament barbed end with low affinity and likely dissociates rapidly from filament barbed ends. We obtained direct evidence from TIRF microscopy that INFT-1 FH1FH2 does not stay on filament barbed end. If INFT-1 is processive, we would have seen filament generated from one spot swings around that spot with immobilized MBP-(INFT-1 FH1FH2) on the slide as shown with several other formins. When MBP-(INFT-1 FH1FH2) is immobilized on the slide, barbed ends grew freely away from their nucleation location. This indicates that MBP-(INFT-1 FH1FH2) does not remain bound to the filament barbed end, similar to another non-processive formin, *Arabidopsis* AFH1. Actin filaments generated by processive formins, such as mouse mDia1 and mDia2 buckle when mDia1 or mDia2 is immobilized on the slide at the barbed end, and at another point with rigor myosin. New actin subunits are inserted between the formin dimers and the barbed end to form a buckle between the formin and myosin attachment points. In our experiments, MBP-(INFT-1 FH1FH2) never buckled filaments when immobilized on a slide together with NEM myosin, even though increased nucleation showed that immobilized INFT-1 was active. These experiments indicate barbed ends do not remain bound to MBP-(INFT-1 FH1FH2) as they grow.

MBP-(INFT-1 FH1FH2) immobilized on spherical beads nucleated filaments with barbed ends directed outward. The 0.5 μM MBP-(INFT-1 FH1FH2) coating the

beads was high comparing to 16 nM used to measure the barbed end elongation rate (Figure 11 and 15).

Excess phosphate decreased barbed end elongation in the presence of INFT-1 FH1FH2 and profilin. The greatest effect was a decrease of 28% in Ce PFN1 versus the barbed end rate in the absence of INFT-1. Extra phosphate in the reaction has been shown to inhibit ɤ-phosphate release from ADP-Pi subunits (Mahaffy and Pollard, 2006). This observation supports the idea that INFT-1 promotes ɤ-phosphate release by subunits at the barbed end, and that ɤ-phosphate release is coupled to formin dissociation. When subunits within a filament are saturated by ɤ-phosphate via an excess of phosphate in solution, INFT-1 dissociation rates, and associated barbed end elongation rates, would decrease. Further study is needed to determine the nature of interaction between INFT-1, profilin, and the nucleotide state of the terminal subunit.

We used an *in vitro* system to reconstitute the actin dynamics mediated by a *C. elegans* inverted formin, INFT-1. INFT-1 FH1FH2 is shown to be non-processive, a property that is unique compared to most other processive formin members. Further study is needed to verify where INFT-1 FH1FH2 is located during actin assembly reaction. Fluorescent labeling of INTF-1 FH1FH2 and two-color TIRF microscopy could be used to determine its position in future experiments.

Eventually we would like to move on to in *vivo* study. We are interested in determining the location of INFT-1 in *C. elegans* cells and finding out its function in particular cell processes. Injection of fluorescent labeled INFT-1 constructs would be a good way to achieve this goal.

INFT-1 C-terminus function has not been studied yet. Formin members like the Diaphanous group own an autoregulatory domain in C-terminus for intermolecular regulation. However, a unique formin INF2 possesses a WASP-homology 2 motif in C-terminus. Although different types of C-terminus in formin members have been discovered, they are all important. We are also curious about the function of INFT-1 C-terminus and want to explore its effect on its N-terminal neighbor and actin.

In all, our study reported an inverted formin INFT-1 from *C. elegans.* INFT-1 has unique domain organization comparing to other, well studied formin family members. INFT-1 lacks the N-terminal regulatory regions and its C terminus is not a homologous of DAD. Thus, INFT-1 cannot be regulated by autoinhibition between DID and DAD domains. The unique domain organization of INFT-1 and lack of homology of the C terminal half to any known protein family implies a new regulation mechanism of formins without DID and DAD. We found that INFT-1 nucleates actin assembly. This characteristic makes INFT-1 a good candidate for regulating actin assembly in *C. elegans*, especially in those cells where INFT-1 has been found to be expressed such as developing neurons, distal tip cells, and the developing vulva. INFT-1 is also non-processive, indicating a new mechanism in formin function on actin assembly. Further comparison of INFT-1 with the other non-processive plant formin, AFH1 could lead to insight into the general mechanism of processivity. INFT-1 also react slightly different in high phosphate buffer, supporting a model where ɤ-phosphate release is affected by formin-meadiated actin assembly. Thus, the study of INFT-1 contributes to the understanding of formin

function and regulation as well as actin assembly process.

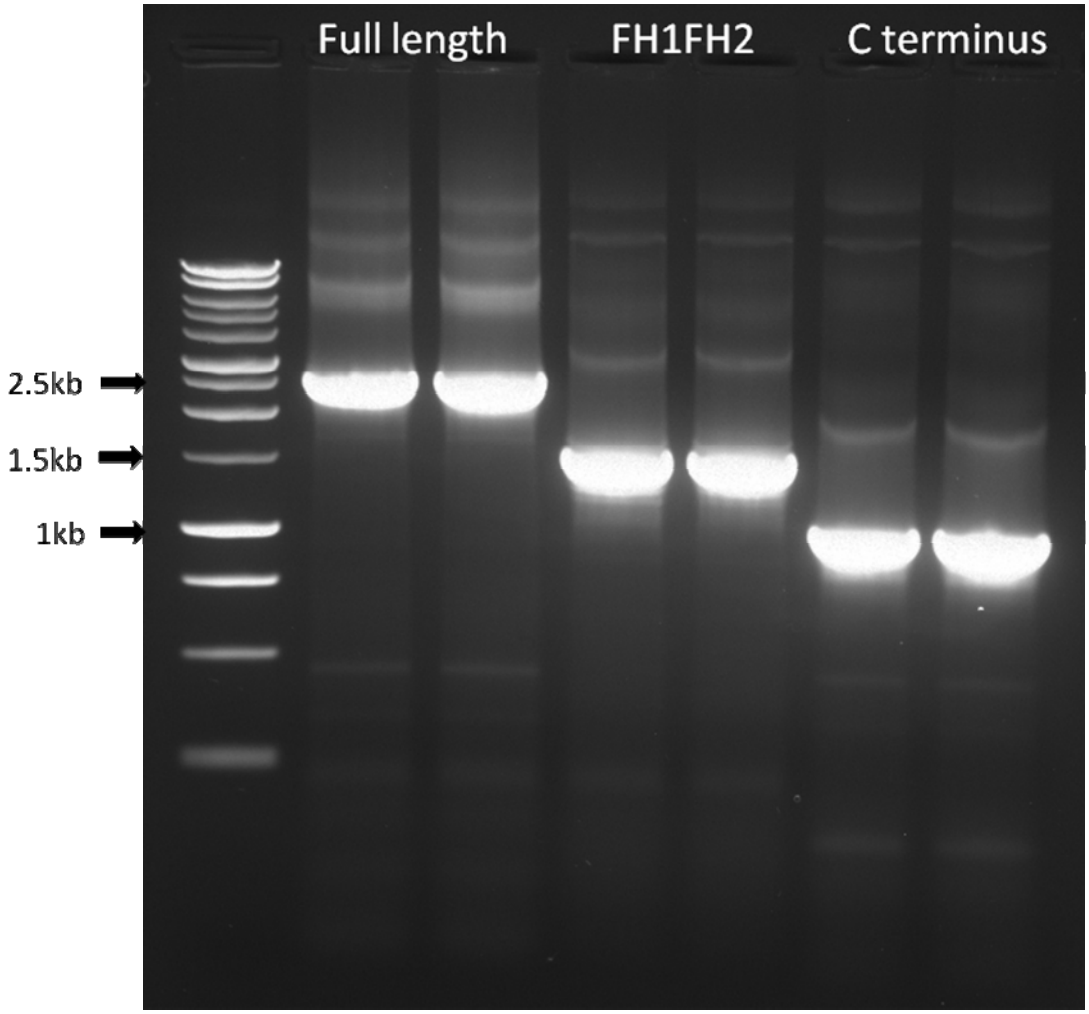

Figure 6 PCR amplification of full length INFT-1, INFT-1 FH1FH2 domains, and INFT-1 C-terminus. The expected size of full length INFT-1 is ~2.5kb, FH1FH2 domain ~1.5kb, C-terminus ~1.0kb. Each reaction has two replicates.

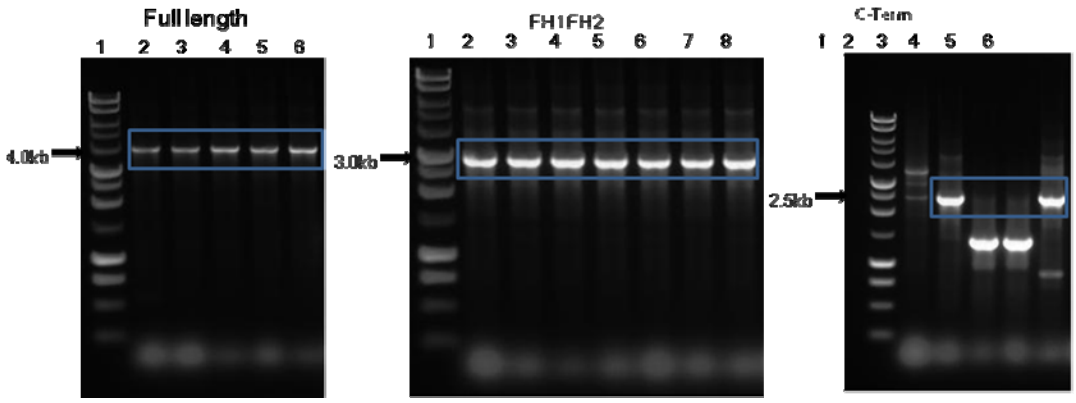

Figure 7 Full-length INFT-1, INFT-1 FH1-FH2 and INFT-1 C-terminus genes were ligated into a modified pET21a vector (an N-term MBP tag followed by a TEV cleavage site and C-term His tag in the vector). Agarose gel electrophoresis shows the expected bands after PCR. Full length ~2.5kb, FH1FH2 domain ~1.5kb, C-terminus ~1.0kb, MBP tag with linker region ~1.5kb.

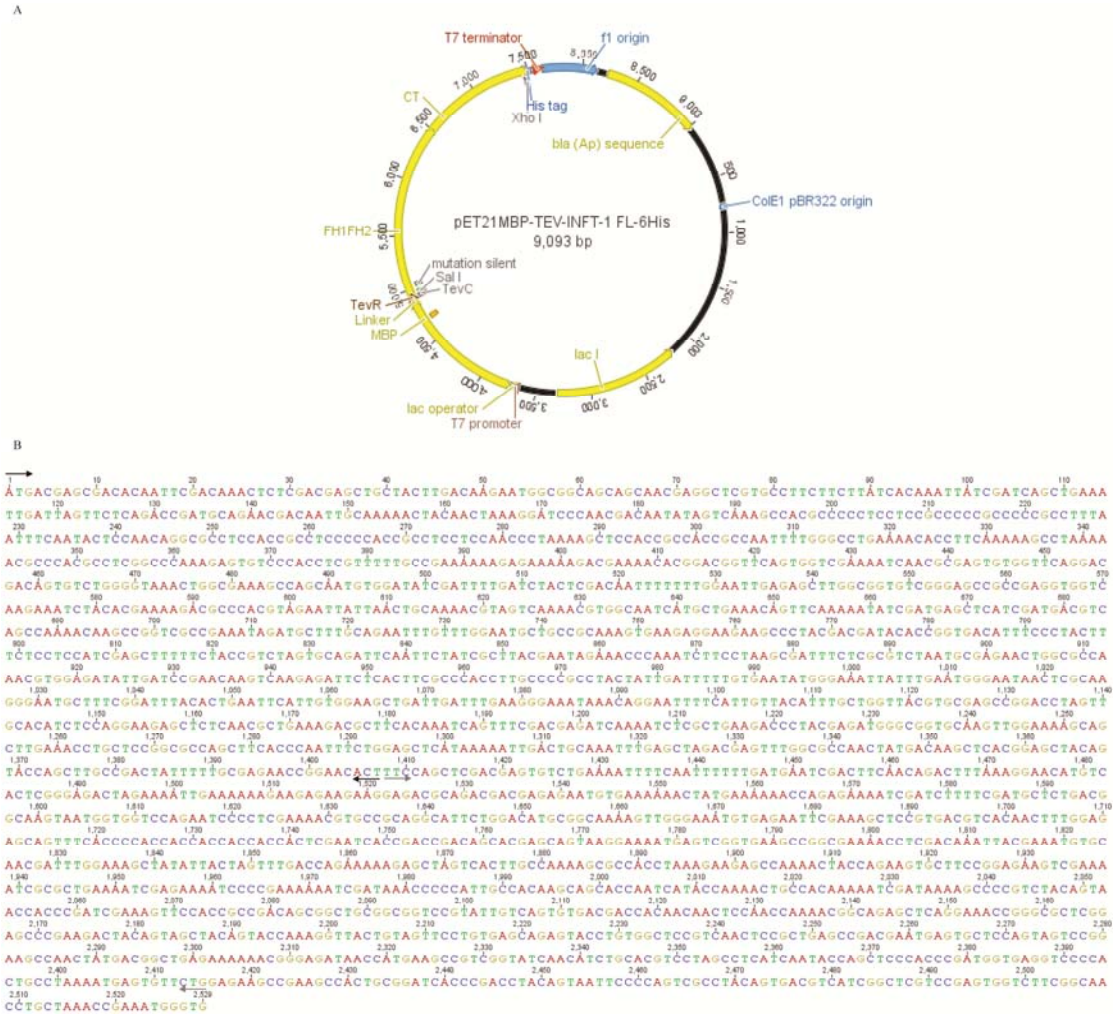

Figure 8 INFT-1 gene sequence. (A) Full length INFT-1 is ligated into a modified pET21a vector. The fragments of FH1FH2 domains and C-terminus are labeled on the vector. (B) Gene sequence of full length INFT-1. INFT-1 FH1FH2 is specified by a pair of black arrows, while the C-terminus is specified by a pair of grey arrows.

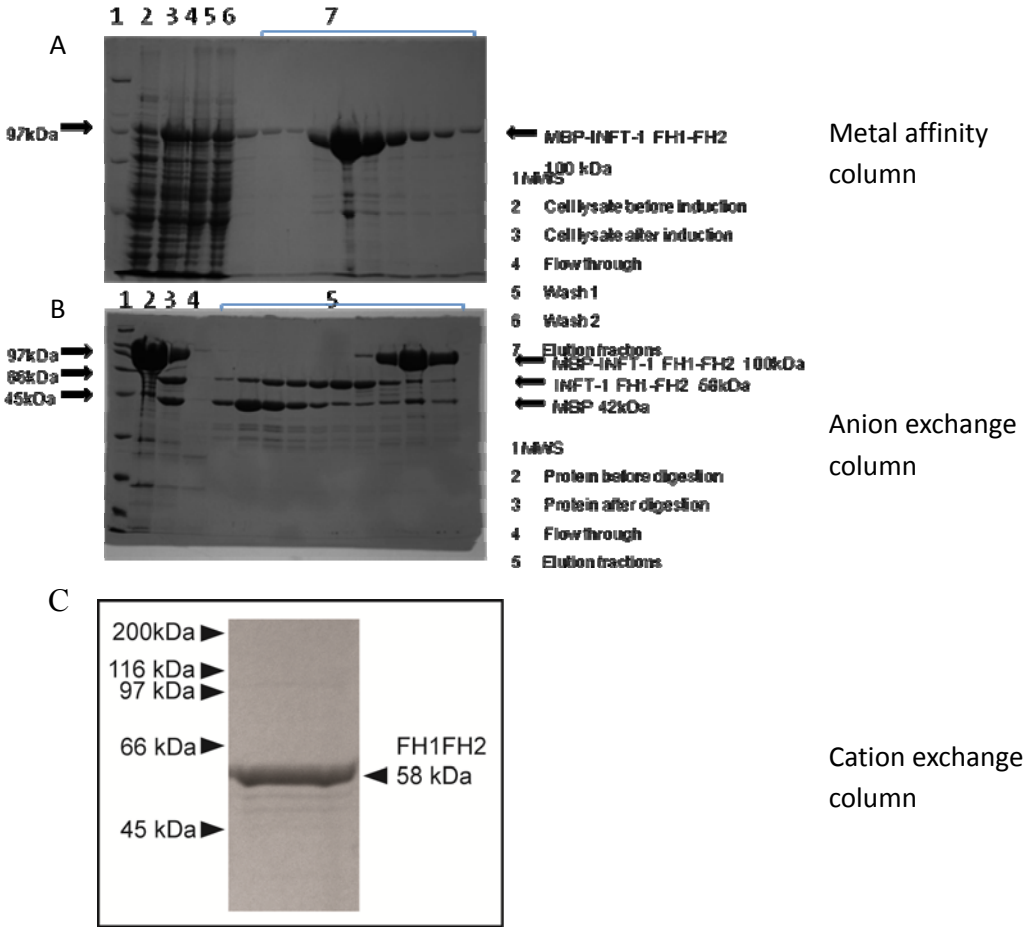

Figure 9 INFT-1 FH1FH2 is purified through a series of chromatography.

(A) Crude cell lysate after induction in lane 3 shows more expression of MBP-(INFT-1 FH1FH2)-6His. (B) INFT-1 FH1FH2-6His is separated from MBP-(INFT-1 FH1FH2)-6His in some fractions. (C) An almost homogeneous band of INFT-1 FH1FH2-6His eluted from a cation exchange column. MBP-(INFT-1 FH1FH2)-6His ~ 100 kDa, INFT-1 FH1FH2-6His ~ 58 kDa, INFT-1 C-terminus ~ 42 kDa.

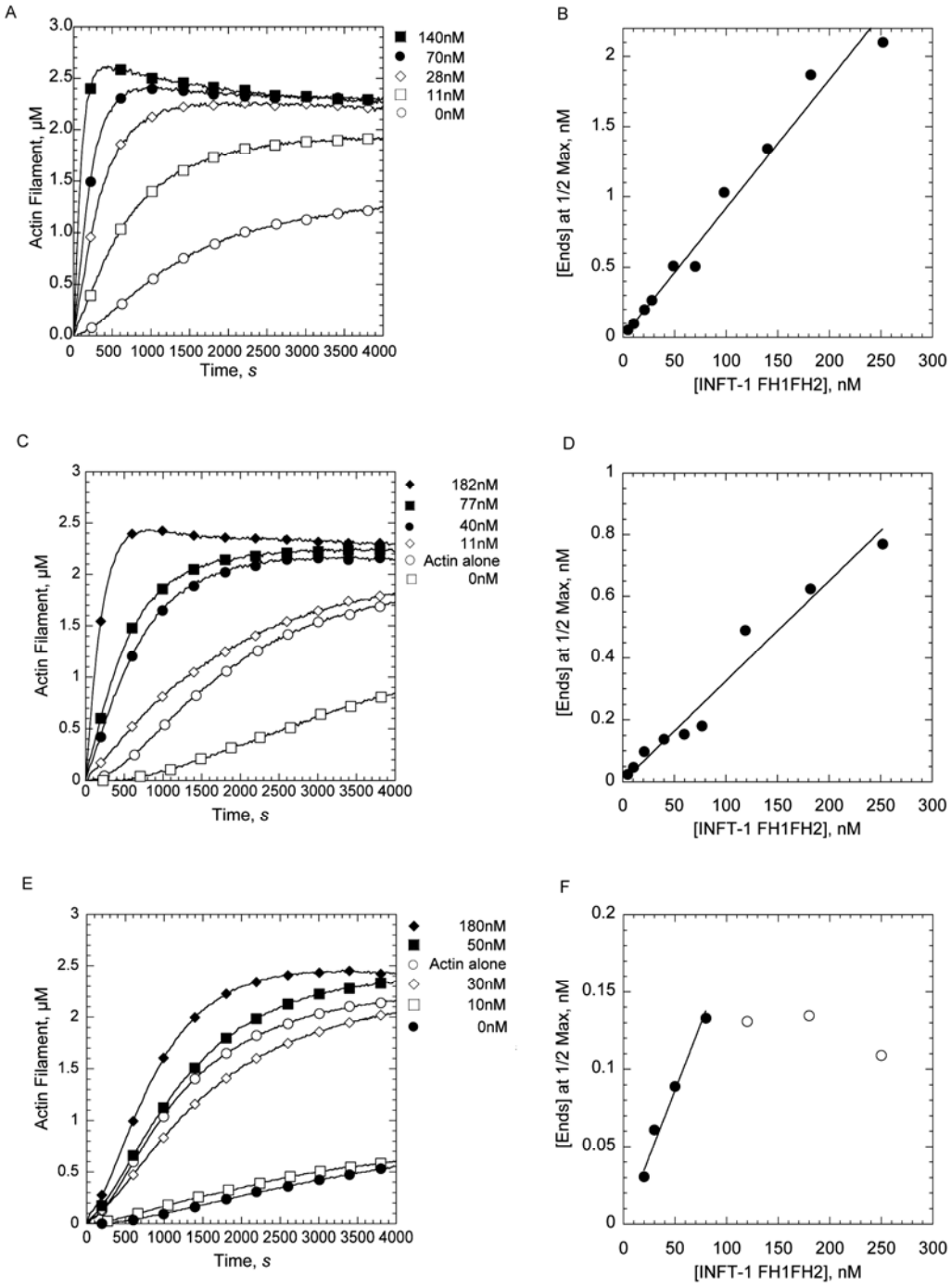
A
Actin Filament, μM
Time, s
140nM
70nM
28nM
11nM
0nM
B
[Ends] at 1/2 Max, nM
[INFT-1 FH1FH2], nM
C
Actin Filament, μM
Time, s
182nM
77nM
40nM
11nM
Actin alone
0nM
D
[Ends] at 1/2 Max, nM
[INFT-1 FH1FH2], nM
E
Actin Filament, μM
Time, s
180nM
50nM
Actin alone
30nM
10nM
0nM
F
[Ends] at 1/2 Max, nM
[INFT-1 FH1FH2], nM

Figure 10 INFT-1 FH1FH2 nucleates actin polymerization.

Conditions: 10 mM Imidazole, pH 7, 50 mM KCl, 1mM $MgCl_2$, 1mM EGTA.

(A) (C) (E) pyrene-actin polymerization assay of 2.5 μM monomeric Mg-ATP actin (20% pyrene labeled).

(B) (D) (F) nucleation efficiency of INFT-1 FH1FH2 in (A) (C) (E), respectively.

(A) pyrene fluorescence over time with actin alone (○), actin plus 11 nM INFT-1 FH1FH2 (□), actin plus 28 nM INFT-1 FH1FH2 (◇), actin plus 70 nM INFT-1 FH1FH2 (●), actin plus 140 nM INFT-1 FH1FH2 (■).

(C) pyrene fluorescence over time with actin alone (○), in the presence of 2.5 μM Hs Profilin without INFT-1 FH1Fh2 (□), with 11 nM INFT-1 FH1FH2 (◇), 40 nM INFT-1 FH1FH2 (●), 77 nM INFT-1 FH1FH2 (■), 182 nM INFT-1 FH1FH2 (◆).

(E) pyrene fluorescence over time with actin alone (○), in the presence of 2.5 μM CePFN-1 without INFT-1 FH1Fh2 (●), with 10 nM INFT-1 FH1FH2 (□), 30 nM INFT-1 FH1FH2 (◇), 50 nM INFT-1 FH1FH2 (■), 180 nM INFT-1 FH1FH2 (◆).

The nucleation efficiency is determined at half-maximum polymerization (Michelot, 2005).

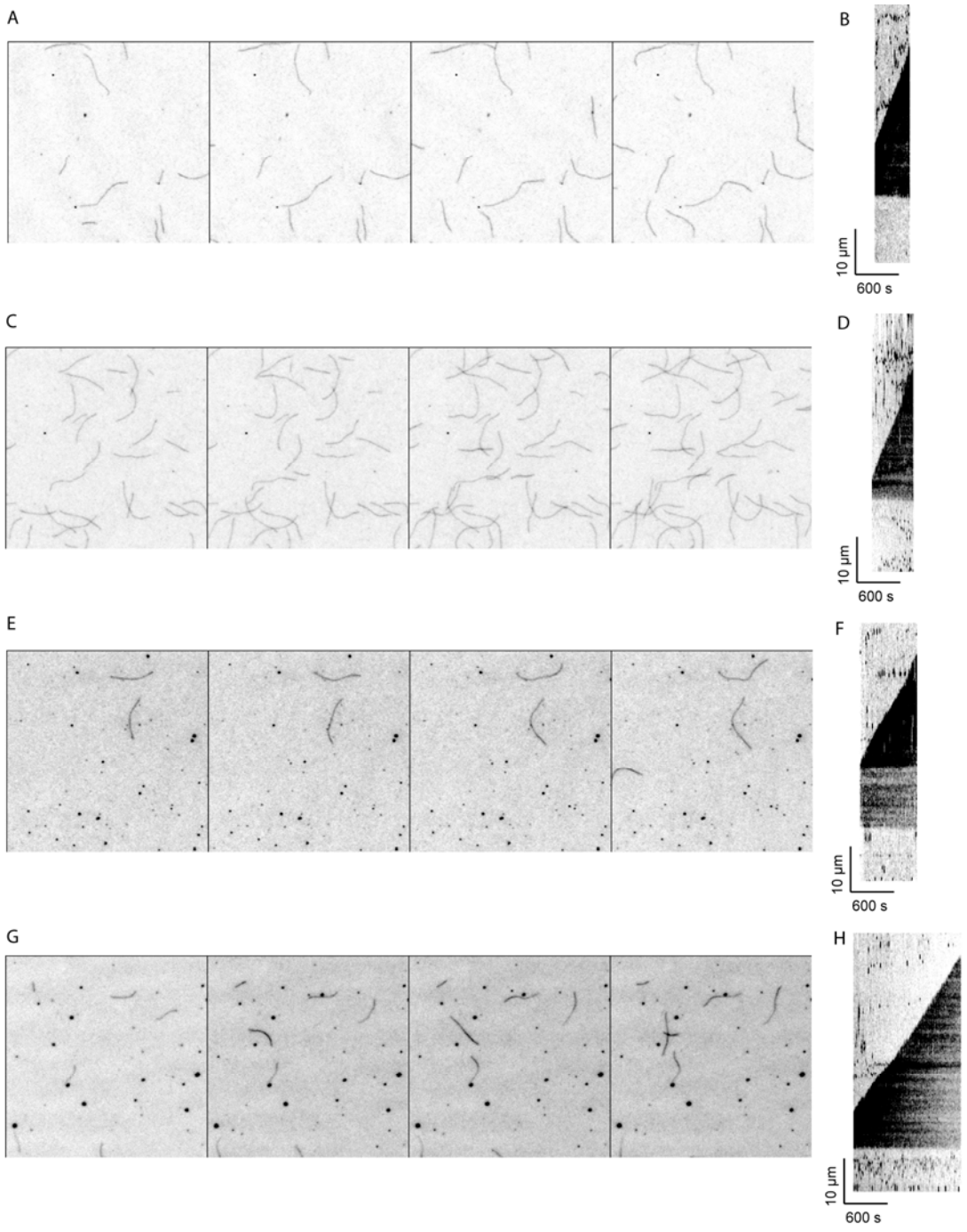
A
B
10 µm
600 s
C
D
10 µm
600 s
E
F
10 µm
600 s
G
H
10 µm
600 s

Figure 11 INFT-1 FH1FH2 dimer enhances Oregon green actin nucleation.

Time lapse total internal reflection fluorescence microscopy of actin assembly in the absence or presence of INFT-1 FH1FH2 and CePFN-1. Assembly of 1 μM ATP-actin with 0.5 μM ATP-actin labeled with Oregon green on slides coated with inactive NEM-Myosin II.

Conditions: 10 mM Imidazole, pH 7, 50 mM KCl, 1mM $MgCl_2$, 1mM EGTA, 100 mM DTT, 0.2 mM ATP, 15 mM glucose, 0.25% methyl cellulose, 20 μg/mL catalase, 100 μg/mL glucose oxidase.

(A) (C) (E) (G) time lapse micrographs with time in min:sec on top left.

(B) (D) (F) (H) kymographs for length of filaments (y-axis) versus time (x-axis).

(A) (B) 1.5 μM actin only

(C) (D) 1.5 μM actin with 16 nM INFT-1 FH1FH2

(E) (F) 1.5 μM actin with 3 μM Ce PFN-1

(G) (H) 1.5 μM actin with 3 μM Ce PFN-1 plus 16 nM INFT-1 FH1FH2

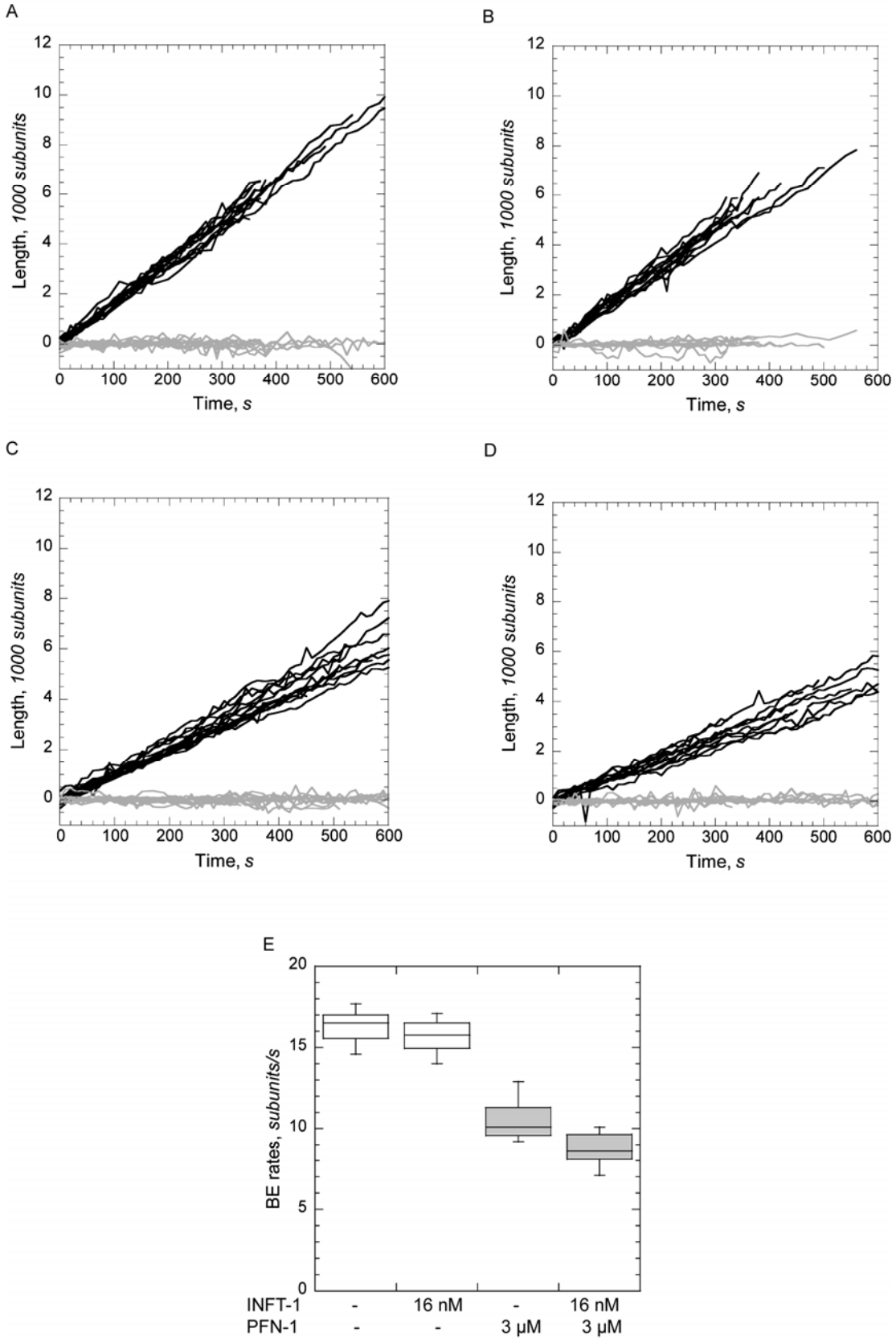
A
B
C
D
E
Length, 1000 subunits
Time, s
BE rates, subunits/s
INFT-1
PFN-1
-
16 nM
3 μM

Figure 12 INFT-1 FH1FH2 slightly slows down barbed end growth rate in the absence of presence of Ce PFN-1. Barbed end elongation rates are 16.4 ± 0.9 subunits/s (n = 20) (A), 15.5 ± 1.1 subunits/s (n = 12) (B), 10.4 ± 1.1 subunits/s (n = 15) (C), 8.7 ± 1.1 subunits/s (n = 11) (D)

Conditions: (A)-(H) 10 mM Imidazole, pH 7, 50 mM KCl, 1mM $MgCl_2$, 1mM EGTA, 100 mM DTT, 0.2 mM ATP, 15 mM glucose, 0.25% methyl cellulose, 20 µg/mL catalase, 100 µg/mL glucose oxidase. (A)- (D), plots of the growth rate for individual filament of barbed (black) and pointed (grey) ends versus time.

(A) 1.5 µM actin only, n=20 from 6 experiments, n is the number of the filaments

(B) 1.5 µM actin with 16 nM INFT-1 FH1FH2, n=12 from 3 experiments

(C) 1.5 µM actin with 3 µM Ce PFN-1, n=15 from 4 experiments

(D) 1.5 µM actin with 3 µM Ce PFN-1 plus 16 nM INFT-1 FH1FH2, n=11 from 3 experiments

(E) boxplot for barbed end growth rates from A-D

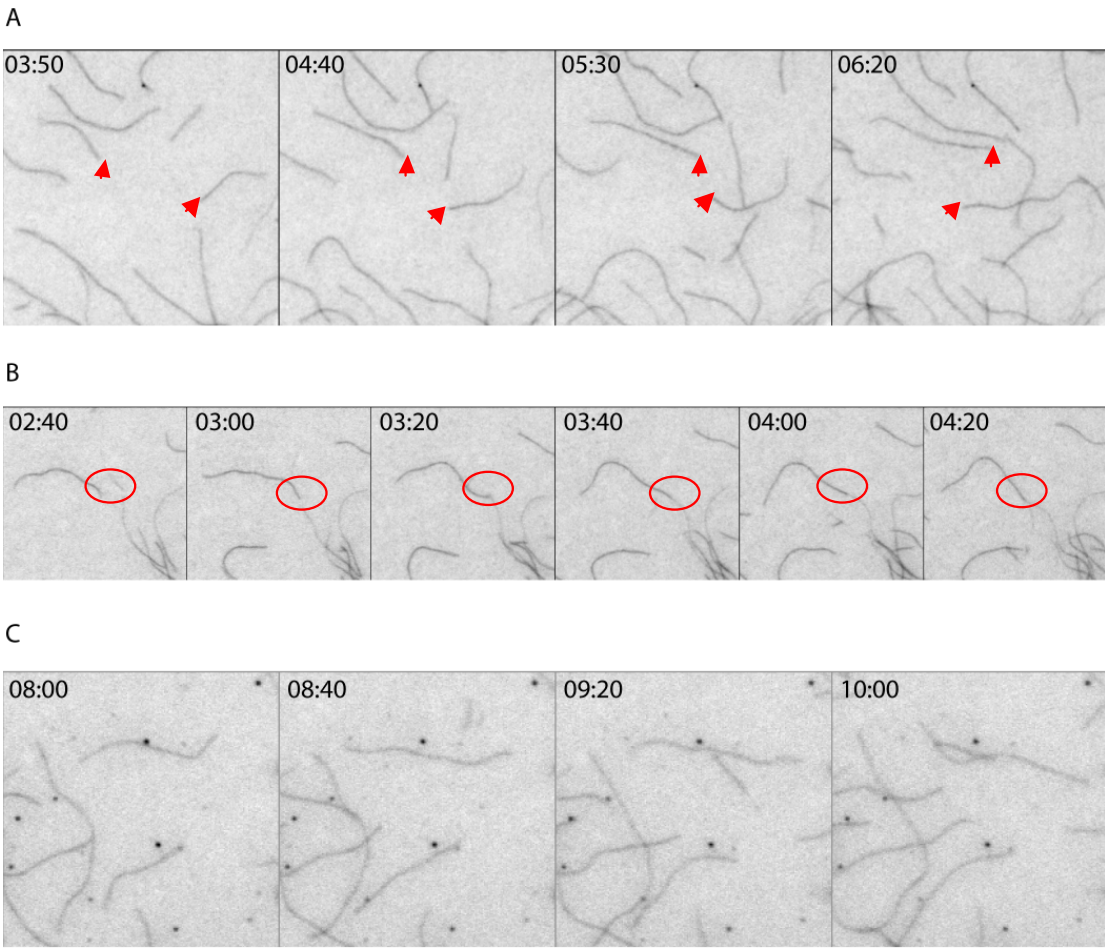

Figure 13. INFT-1 is a non-processive formin. Conditions: 10 mM Imidazole, pH 7, 50 mM KCl, 1mM $MgCl_2$, 1mM EGTA, 100 mM DTT, 0.2 mM ATP, 15 mM glucose, 0.25% methyl cellulose, 20 µg/mL catalase, 100 µg/mL glucose oxidase.

(A) Assembly of 1 µM ATP-actin with 0.5 µM ATP-actin labeled with Oregon green on slides coated with MBP-(INFT-1 FH1FH2). Filament barbed ends do not stick to one spot on the slide. However, they are moving freely. Red arrows, barbed ends.

(B) Annealing events (circled out by red ovals) occurred frequently from the same movie shown in (A).

(C) Assembly of 1 µM ATP-actin with 0.5 µM ATP-actin labeled with Oregon green on slides coated with both MBP-(INFT-1 FH1FH2) and inactive NEM myosin II.

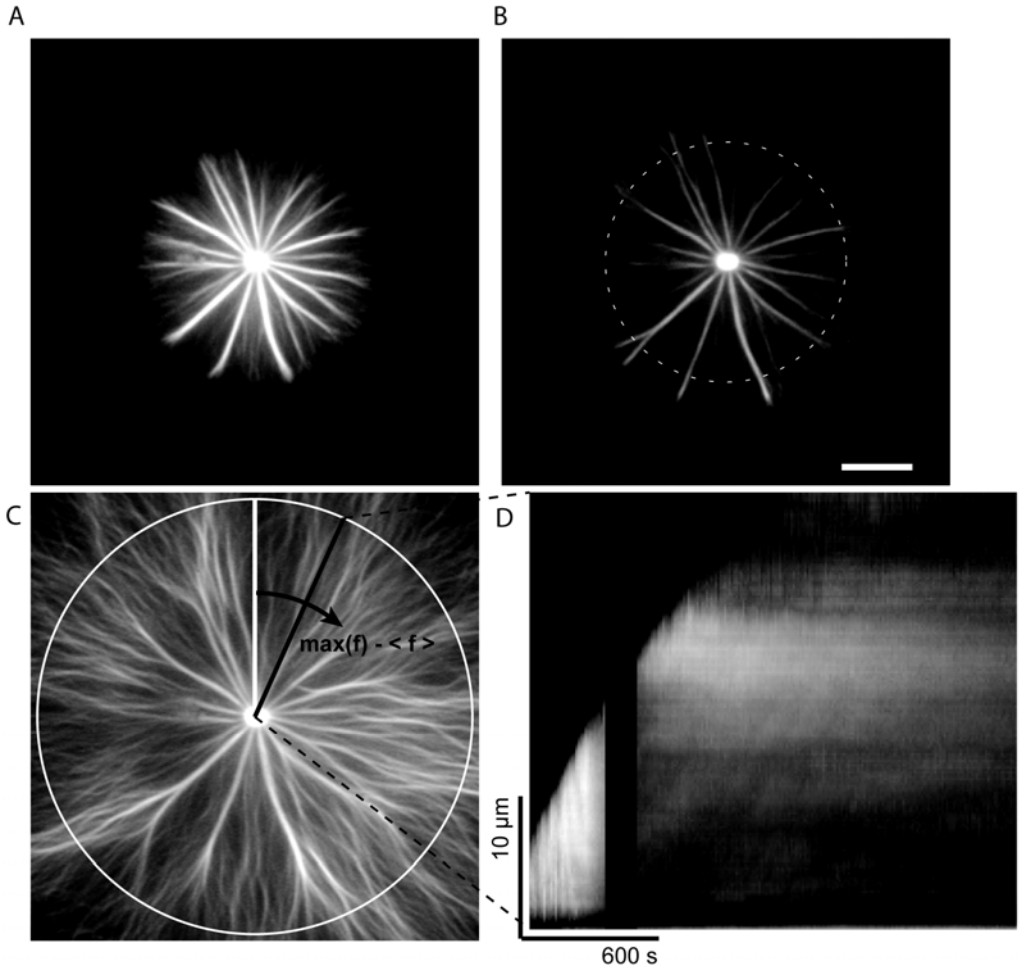
A
B
C
D
max(f) - < f >
10 µm
600 s

Figure 14: Actin bundles form around MBP-INFT-1 FH1FH2 coated spherical beads. Conditions: 10 mM Imidazole, pH 7, 50 mM KCl, 1mM $MgCl_2$, 1mM EGTA, 100 mM DTT, 0.2 mM ATP, 15 mM glucose, 0.25% methyl cellulose, 20 μg/mL catalase, 100 μg/mL glucose oxidase. Spherical bead was coated with 2 μM MBP-(INFT-1 FH1FH2). Its diameter is 0.5 micron. (A) Original image of the actin filaments and bundles.

(B)The dashed circle shows when we start the photobleaching.

(C) The filament with the maximum fluorescence intensity in each frame was determined and the length of each filament is shown in a kymograph in (D).

(D) The length of the filament with the maximum fluorescence intensity is plotted against time. The black gap between the two bright parts is where we did photobleaching to the reaction.

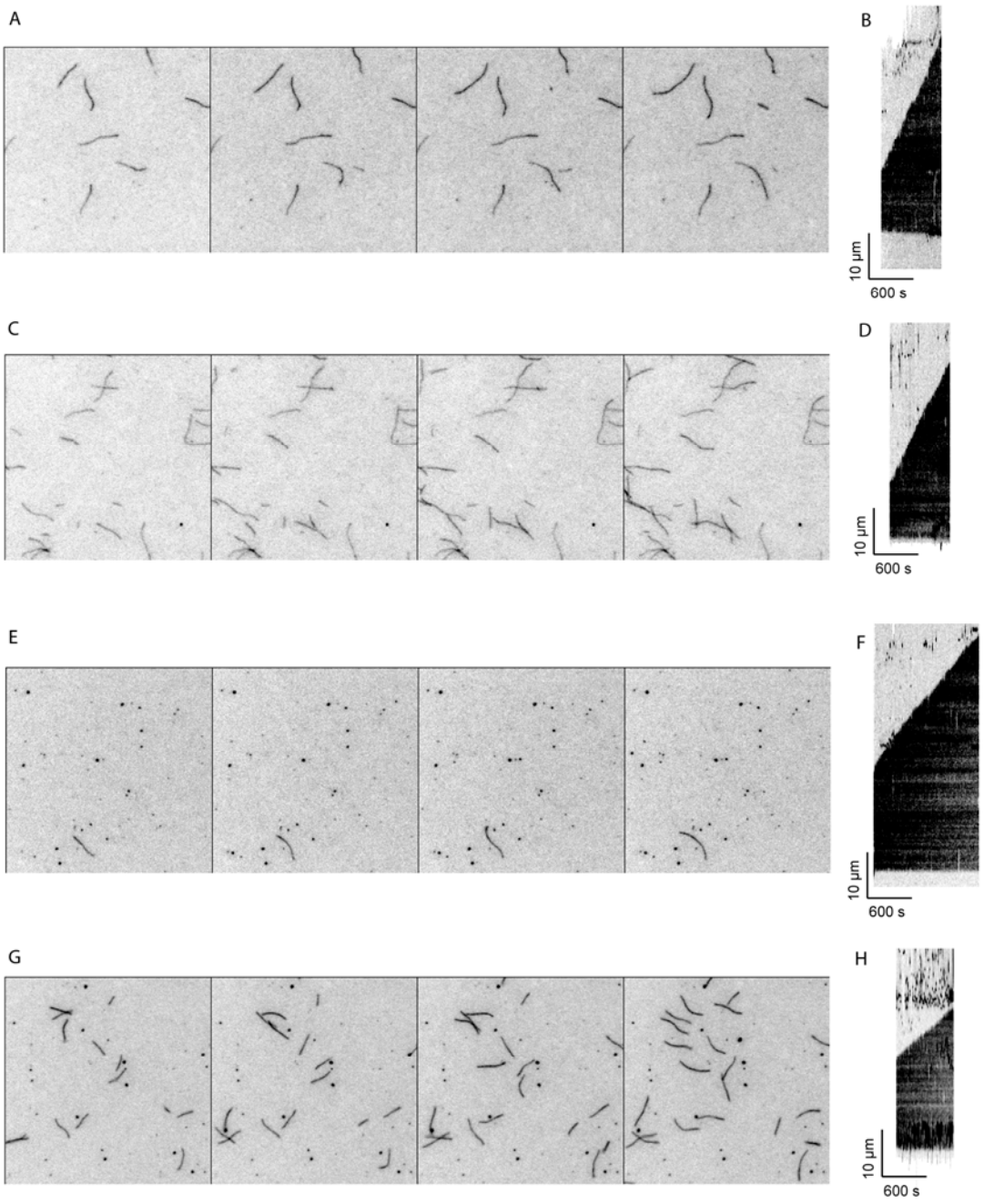
A
B
10 µm
600 s
C
D
10 µm
600 s
E
F
10 µm
600 s
G
H
10 µm
600 s

Figure 15 INFT-1 FH1FH2 mediated actin assembly is affected by excess phosphate. Time lapse total internal reflection fluorescence microscopy of actin assembly in the absence or presence of INFT-1 FH1FH2 and CePFN-1 in high phosphate condition. Assembly of 1 μM ATP-actin with 0.5 μM ATP-actin labeled with Oregon green on slides coated with inactive NEM-Myosin II.

(A) (C) (E) (G) time lapse micrographs with time in min:sec on top left.

(B) (D) (F) (H) kymographs for length of filaments (y-axis) versus time (x-axis).

Conditions: 10 mM Imidazole, pH 7, 50 mM K^+, 25 mM PO_4^-, 1mM $MgCl_2$, 1mM EGTA, 100 mM DTT, 0.2 mM ATP, 15 mM glucose, 0.25% methyl cellulose, 20 μg/mL catalase, 100 μg/mL glucose oxidase.

(A) (B) 1.5 μM actin only

(C) (D) 1.5 μM actin with 16 nM INFT-1 FH1FH2

(E) (F) 1.5 μM actin with 3 μM Ce PFN-1

(G) (H) 1.5 μM actin with 3 μM Ce PFN-1 plus 16 nM INFT-1 FH1FH2

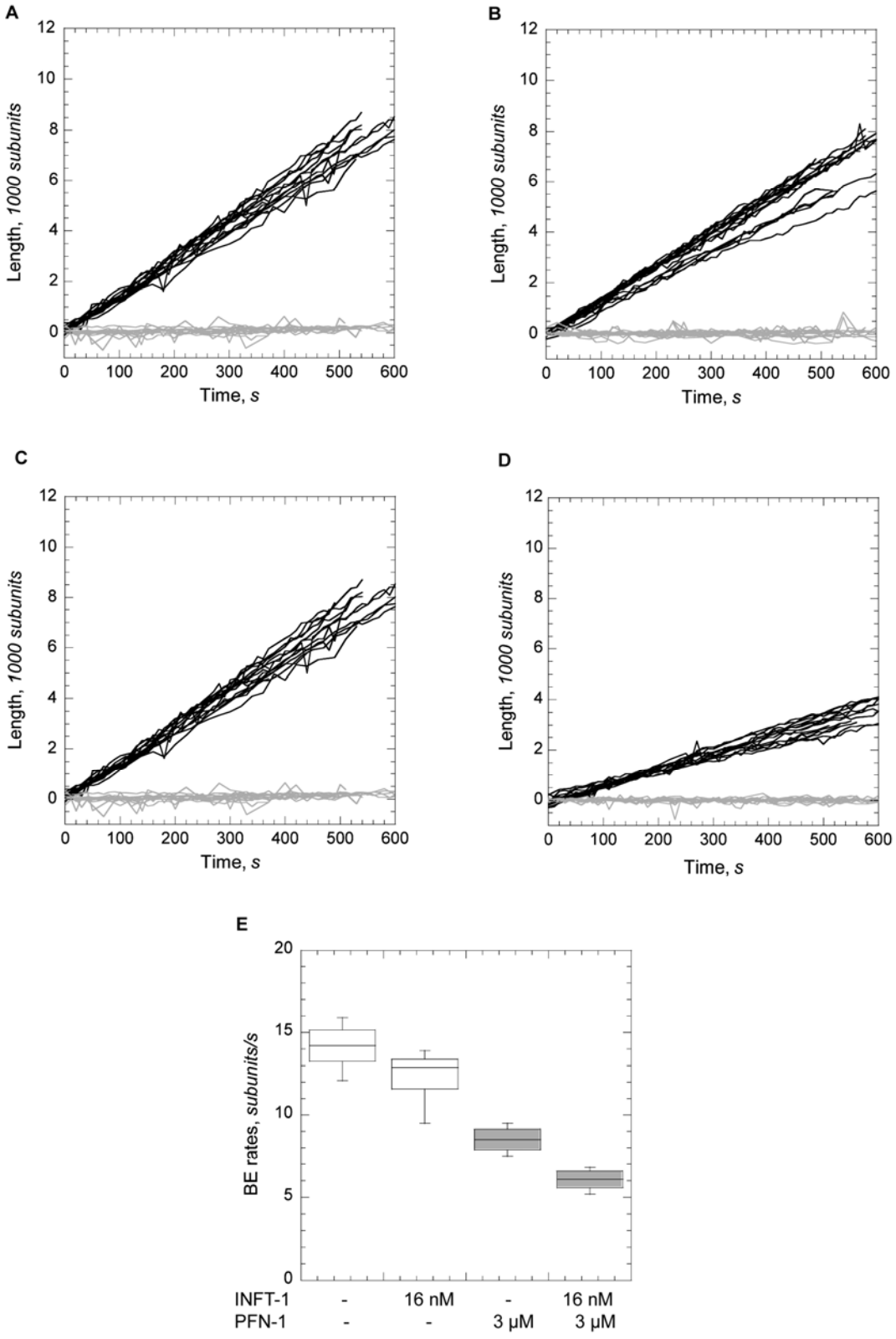
A
B
C
D
E
Length, 1000 subunits
Time, s
BE rates, subunits/s
INFT-1 - 16 nM - 16 nM
PFN-1 - - 3 μM 3 μM

Figure 16 INFT-1 FH1FH2 has a greater effect on slowing down barbed end growth in the presence of excess phosphate. (A) (B) (C) and (D) show the rates for the reactions in Figure 15 (A) (C) (E) and (G) respectively. (A): 14.1 ± 1.1 subunits/s; (B): 12.4 ± 1.3 subunits/s; (C): 8.5 ± 0.7 subunits/s; (D): 6.1 ± 0.5 subunits/s. E: boxplot to compare the four rates.

Conditions: 10 mM Imidazole, pH 7, 50 mM K^+, 25 mM PO_4^-, 1mM $MgCl_2$, 1mM EGTA, 100 mM DTT, 0.2 mM ATP, 15 mM glucose, 0.25% methyl cellulose, 20 μg/mL catalase, 100 μg/mL glucose oxidase.

(A) 1.5 μM actin only, n=15 from 5 experiments, n is the number of the filaments

(B) 1.5 μM actin with 16 nM INFT-1 FH1FH2, n=19 from 5 experiments

(C) 1.5 μM actin with 3 μM Ce PFN-1, n=11 from 3 experiments

(D) 1.5 μM actin with 3 μM Ce PFN-1 plus 16 nM INFT-1 FH1FH2, n=14 from 4 experiments

(E) boxplot for barbed end growth rates from A-D

References

Alberts, A.S. 2001. Identification of a carboxyl-terminal diaphanous-related formin homology protein autoregulatory domain. J Biol Chem. 276:2824-30.

Albertson, T.E., A. Dawson, F. de Latorre, R.S. Hoffman, J.E. Hollander, A. Jaeger, W.R. Kerns, 2nd, T.G. Martin, and M.P. Ross. 2001. TOX-ACLS: toxicologic-oriented advanced cardiac life support. *Ann Emerg Med*. 37:S78-90.

Brandt, D. T. *et al.* 2007 Dia1 and IQGAP1 interact in cell migration and phagocytic cup formation. *J. Cell Biol.***178**, 193–200

Campellone K. G. and Welch M. D. 2010 A nucleator arms race: cellular control of actin assembly. *Nature Rev. Mol. Cell Biol.***11**, 237–251

Castrillon, D.H., and S.A. Wasserman. 1994. Diaphanous is required for cytokinesis in Drosophila and shares domains of similarity with the products of the limb deformity gene. *Development*. 120:3367-77.

Chang, F., D. Drubin, and P. Nurse. 1997. cdc12p, a protein required for cytokinesis in fission yeast, is a component of the cell division ring and interacts with profilin. *J Cell Biol*. 137:169-82.

Chereau D., Boczkowska M., Skwarek-Maruszewska A., Fujiwara I., Hayes D.B., Rebowski G., Lappalainen P., Pollard T.D., Dominguez R. 2008 Leiomodin is an actin filament nucleator in muscle cells, *Science* 320: 239–243

Chesarone, M. A., DuPage, A. G. & Goode, B. L. 2010 Unleashing formins to remodel the actin and microtubule cytoskeletons. *Nature Rev. Mol. Cell Biol.***11**,

62–74

Chesarone, M., Gould, C. J., Moseley, J. B. & Goode, B. L. 2009 Displacement of formins from growing barbed ends by Bud14 is critical for actin cable architecture and function. *Dev. Cell* **16**, 292–302

Cheung, A.Y., and H.M. Wu. 2004. Overexpression of an Arabidopsis formin stimulates supernumerary actin cable formation from pollen tube cell membrane. *Plant Cell*. 16:257-69.

Chhabra, E. S., Ramabhadran, V., Gerber, S. A. & Higgs, H. N. 2009 INF2 is an endoplasmic reticulumassociated formin protein. *J. Cell Sci.* **122**, 1430–1440

Chhabra, E.S., and H.N. Higgs. 2006. INF2 Is a WASP homology 2 motif-containing formin that severs actin filaments and accelerates both polymerization and depolymerization. *J Biol Chem*. 281:26754-67.

Echard, A. 2004. [Dissecting cytokinesis: proteomic and genomic approaches]. *Med Sci (Paris)*. 20:845-6.

Eisenmann, K. M. *et al.* 2007 Dia-interacting protein modulates formin-mediated actin assembly at the cell cortex. *Curr. Biol.* **17**, 579–591

Emmons, S., H. Phan, J. Calley, W. Chen, B. James, and L. Manseau. 1995. Cappuccino, a Drosophila maternal effect gene required for polarity of the egg and embryo, is related to the vertebrate limb deformity locus. *Genes Dev*. 9:2482-94.

Evangelista, M., D. Pruyne, D.C. Amberg, C. Boone, and A. Bretscher. 2002. Formins direct Arp2/3-independent actin filament assembly to polarize cell growth in

yeast. *Nat Cell Biol*. 4:260-9.

Faix, J., and R. Grosse. 2006. Staying in shape with formins. *Dev Cell*. 10:693-706.

Goode, B.L., and M.J. Eck. 2007. Mechanism and function of formins in the control of actin assembly. *Annu Rev Biochem*. 76:593-627.

Grunt M, Zárský V., Cvrcková F. 2008 Roots of angiosperm formins: the evolutionary history of plant FH2 domain-containing proteins, *BMC Evol. Biol.* 8: 115.

Habas, R., Y. Kato, and X. He. 2001. Wnt/Frizzled activation of Rho regulates vertebrate gastrulation and requires a novel Formin homology protein Daam1. *Cell*. 107:843-54.

Harris, E.S., F. Li, and H.N. Higgs. 2004. The mouse formin, FRLalpha, slows actin filament barbed end elongation, competes with capping protein, accelerates polymerization from monomers, and severs filaments. *J Biol Chem*. 279:20076-87.

Harris, E.S., I. Rouiller, D. Hanein, and H.N. Higgs. 2006. Mechanistic differences in actin bundling activity of two mammalian formins, FRL1 and mDia2. *J Biol Chem*. 281:14383-92.

Higgs, H.N. 2005. Formin proteins: a domain-based approach. *Trends Biochem Sci*. 30:342-53.

Higgs, H.N., and K.J. Peterson. 2005. Phylogenetic analysis of the formin homology 2 domain. *Mol Biol Cell*. 16:1-13.

Hotulainen, P., and P. Lappalainen. 2006. Stress fibers are generated by two distinct actin assembly mechanisms in motile cells. *J Cell Biol*. 173:383-94.

Hunt-Newbury, R., R. Viveiros, R. Johnsen, A. Mah, D. Anastas, L. Fang, E. Halfnight, D. Lee, J. Lin, A. Lorch, S. McKay, H.M. Okada, J. Pan, A.K. Schulz, D. Tu, K. Wong, Z. Zhao, A. Alexeyenko, T. Burglin, E. Sonnhammer, R. Schnabel, S.J. Jones, M.A. Marra, D.L. Baillie, and D.G. Moerman. 2007. High-throughput in *vivo* analysis of gene expression in Caenorhabditis elegans. *PLoS Biol*. 5:e237.

Imamura, H., K. Tanaka, T. Hihara, M. Umikawa, T. Kamei, K. Takahashi, T. Sasaki, and Y. Takai. 1997. Bni1p and Bnr1p: downstream targets of the Rho family small G-proteins which interact with profilin and regulate actin cytoskeleton in Saccharomyces cerevisiae. *EMBO J*. 16:2745-55.

Ingouff, M., J.N. Fitz Gerald, C. Guerin, H. Robert, M.B. Sorensen, D. Van Damme, D. Geelen, L. Blanchoin, and F. Berger. 2005. Plant formin AtFH5 is an evolutionarily conserved actin nucleator involved in cytokinesis. *Nat Cell Biol*. 7:374-80.

Johnston, R.J., Jr., J.W. Copeland, M. Fasnacht, J.F. Etchberger, J. Liu, B. Honig, and O. Hobert. 2006. An unusual Zn-finger/FH2 domain protein controls a left/right asymmetric neuronal fate decision in C. elegans. *Development*. 133:3317-28.

Kobielak, A., H.A. Pasolli, and E. Fuchs. 2004. Mammalian formin-1 participates in adherens junctions and polymerization of linear actin cables. *Nat Cell Biol*. 6:21-30.

Kovar, D.R., E.S. Harris, R. Mahaffy, H.N. Higgs, and T.D. Pollard. 2006. Control of the assembly of ATP- and ADP-actin by formins and profilin. *Cell*. 124:423-35.

Kovar, D.R., J.R. Kuhn, A.L. Tichy, and T.D. Pollard. 2003. The fission yeast cytokinesis formin Cdc12p is a barbed end actin filament capping protein gated by profilin. *J Cell Biol*. 161:875-87.

Kovar, D.R., and T.D. Pollard. 2004. Insertional assembly of actin filament barbed ends in association with formins produces piconewton forces. *Proc Natl Acad Sci U S A*. 101:14725-30.

Kozlov, M.M., and A.D. Bershadsky. 2004. Processive capping by formin suggests a force-driven mechanism of actin polymerization. *J Cell Biol*. 167:1011-7.

Kuhn J.R**.** and Pollard T.D., 2005 Real time measurements of actin filament polymerization by total internal reflection fluorescence microscopy. **Biophys. J.** 88: 1387-1402

Lammers, M., R. Rose, A. Scrima, and A. Wittinghofer. 2005. The regulation of mDia1 by autoinhibition and its release by Rho*GTP. *EMBO J*. 24:4176-87.

Li, F., and H.N. Higgs. 2003. The mouse Formin mDia1 is a potent actin nucleation factor regulated by autoinhibition. *Curr Biol*. 13:1335-40.

Li, F., and H.N. Higgs. 2005. Dissecting requirements for auto-inhibition of actin nucleation by the formin, mDia1. *J Biol Chem*. 280:6986-92.

Lu, J. and Pollard, T.D. 2001 Profilin binding to poly-L-proline and actin monomers along with ability to catalyze actin nucleotide exchange is required for viability of fission yeast. *Mol. Biol. Cell* 12: 1161–1175

Mallavarapu, A., and T. Mitchison. 1999. Regulated actin cytoskeleton assembly at filopodium tips controls their extension and retraction. *J Cell Biol*. 146:1097-106.

Maltzman, T., K. Knoll, M.E. Martinez, T. Byers, B.R. Stevens, J.R. Marshall, M.E. Reid, J. Einspahr, N. Hart, A.K. Bhattacharyya, C.B. Kramer, R. Sampliner, D.S. Alberts, and D.J. Ahnen. 2001. Ki-ras proto-oncogene mutations in sporadic colorectal adenomas: relationship to histologic and clinical characteristics. *Gastroenterology*. 121:302-9.

Martin, S.G., W.H. McDonald, J.R. Yates, 3rd, and F. Chang. 2005. Tea4p links microtubule plus ends with the formin for3p in the establishment of cell polarity. *Dev Cell*. 8:479-91.

Matsuda K., Matsuda S., Gladding C.M., Yuzaki M. 2006 Characterization of the delta2 glutamate receptor-binding protein delphilin: splicing variants with differential palmitoylation and an additional PDZ domain, *J. Biol. Chem.* 281: 25577–25587.

Matusek, T., A. Djiane, F. Jankovics, D. Brunner, M. Mlodzik, and J. Mihaly. 2006. The Drosophila formin DAAM regulates the tracheal cuticle pattern through organizing the actin cytoskeleton. *Development*. 133:957-66.

Michelot A., Derivery E., Paterski-Boujemaa R., Guerin C., Huang S., Parcy F., Staiger C.J., Blanchoin L. 2006 A novel mechanism for the formation of actin-filament bundles by a nonprocessive formin, *Curr. Biol.* 16: 1924–1930.

Michelot A. 2005 The formin homology 1 domain modulates the actin nucleation and bundling activity of *Arabidopsis* FORMIN1. *Plant Cell* **17:** 2296–2313

Miyagi Y., Yamashita T., Fukaya M., Sonoda T., Okuno T., Yamada K., Watanabe M.,Nagashima Y., Aoki I., Okuda K., Mishina M., Kawamoto S. 2002 Delphilin:

a novel PDZ and formin homology domain-containing protein that synaptically colocalizes and interacts with glutamate receptor delta 2 subunit, *J. Neurosci.* 22: 803–814.

Moseley, J.B., I. Sagot, A.L. Manning, Y. Xu, M.J. Eck, D. Pellman, and B.L. Goode. 2004. A conserved mechanism for Bni1- and mDia1-induced actin assembly and dual regulation of Bni1 by Bud6 and profilin. *Mol Biol Cell*. 15:896-907.

Nakano, K., K. Takaishi, A. Kodama, A. Mammoto, H. Shiozaki, M. Monden, and Y. Takai. 1999. Distinct actions and cooperative roles of ROCK and mDia in Rho small G protein-induced reorganization of the actin cytoskeleton in Madin-Darby canine kidney cells. *Mol Biol Cell*. 10:2481-91.

Neidt, E. M., Scott, B. J. & Kovar, D. R. 2009 Formin differentially utilizes profilin isoforms to rapidly assemble actin filaments. *J. Biol. Chem.* **284**: 673–684.

Neidt, E.M., C.T. Skau, and D.R. Kovar. 2008. The cytokinesis formins from the nematode worm and fission yeast differentially mediate actin filament assembly. *J Biol Chem*. 283:23872-83.

Nezami, A.G., F. Poy, and M.J. Eck. 2006. Structure of the autoinhibitory switch in formin mDia1. *Structure*. 14:257-63.

Ono, S. 1999. Purification and biochemical characterization of actin from Caenorhabditis elegans: its difference from rabbit muscle actin in the interaction with nematode ADF/cofilin. *Cell Motil Cytoskeleton*. 43:128-36.

Otomo, T., C. Otomo, D.R. Tomchick, M. Machius, and M.K. Rosen. 2005a. Structural basis of Rho GTPase-mediated activation of the formin mDia1. *Mol*

Cell. 18:273-81.

Otomo, T., D.R. Tomchick, C. Otomo, S.C. Panchal, M. Machius, and M.K. Rosen. 2005b. Structural basis of actin filament nucleation and processive capping by a formin homology 2 domain. *Nature*. 433:488-94.

Paul, A.S., and T.D. Pollard. 2008. The role of the FH1 domain and profilin in formin-mediated actin-filament elongation and nucleation. *Curr Biol*. 18:9-19.

Pellegrin, S., and H. Mellor. 2005. The Rho family GTPase Rif induces filopodia through mDia2. *Curr Biol*. 15:129-33.

Peng, J., B.J. Wallar, A. Flanders, P.J. Swiatek, and A.S. Alberts. 2003. Disruption of the Diaphanous-related formin Drf1 gene encoding mDia1 reveals a role for Drf3 as an effector for Cdc42. *Curr Biol*. 13:534-45.

Polet, D., Lambrechts, A., Ono, K., Mah, A., Peelman, F., Vandekerckhove, J., Baillie, D. L., Ampe, C., and Ono, S. 2006 *Caenorhabditis elegans* expresses three functional profilins in a tissue-specific manner. *Cell Motil. Cytoskeleton* 63: 14–28

Pollard, T.D., L. Blanchoin, and R.D. Mullins. 2000. Molecular mechanisms controlling actin filament dynamics in nonmuscle cells. *Annu Rev Biophys Biomol Struct*. 29:545-76.

Pollard, T. D. (2007). "Regulation of actin filament assembly by Arp2/3 complex and formins." *Annu Rev Biophys Biomol Struct* **36**: 451-477.

Pollard, T.D., and J.A. Cooper. 1986. Actin and actin-binding proteins. A critical evaluation of mechanisms and functions. *Annu Rev Biochem*. 55:987-1035.

Pollard, T.D. 1984 Polymerization of ADP-actin. J. Cell Biol. 99:769-777

Pring, M., M. Evangelista, C. Boone, C. Yang, and S.H. Zigmond. 2003. Mechanism of formin-induced nucleation of actin filaments. *Biochemistry*. 42:486-96.

Pruyne, D., M. Evangelista, C. Yang, E. Bi, S. Zigmond, A. Bretscher, and C. Boone. 2002. Role of formins in actin assembly: nucleation and barbed-end association. *Science*. 297:612-5.

Quinlan, M. E., Hilgert, S., Bedrossian, A., Mullins, R. D. & Kerkhoff, E. 2007 Regulatory interactions between two actin nucleators, Spire and Cappuccino. *J. Cell Biol.***179**, 117–128

Renault L., Bugyi B., Carlier M.F. 2008 Spire and Cordon-bleu: multifunctional regulators of actin dynamics, *Trends Cell Biol.* 18: 494–504

Rivero, F., T. Muramoto, A.K. Meyer, H. Urushihara, T.Q. Uyeda, and C. Kitayama. 2005. A comparative sequence analysis reveals a common GBD/FH3-FH1-FH2-DAD architecture in formins from Dictyostelium, fungi and metazoa. *BMC Genomics*. 6:28.

Romero, S., C. Le Clainche, D. Didry, C. Egile, D. Pantaloni, and M.F. Carlier. 2004. Formin is a processive motor that requires profilin to accelerate actin assembly and associated ATP hydrolysis. *Cell*. 119:419-29.

Rose, R., M. Weyand, M. Lammers, T. Ishizaki, M.R. Ahmadian, and A. Wittinghofer. 2005. Structural and mechanistic insights into the interaction between Rho and mammalian Dia. *Nature*. 435:513-8.

Sagot, I., S.K. Klee, and D. Pellman. 2002a. Yeast formins regulate cell polarity by

controlling the assembly of actin cables. *Nat Cell Biol*. 4:42-50.

Sagot, I., A.A. Rodal, J. Moseley, B.L. Goode, and D. Pellman. 2002b. An actin nucleation mechanism mediated by Bni1 and profilin. *Nat Cell Biol*. 4:626-31.

Sahai, E., and C.J. Marshall. 2002. ROCK and Dia have opposing effects on adherens junctions downstream of Rho. *Nat Cell Biol*. 4:408-15.

Schirenbeck, A., R. Arasada, T. Bretschneider, M. Schleicher, and J. Faix. 2005a. Formins and VASPs may co-operate in the formation of filopodia. *Biochem Soc Trans*. 33:1256-9.

Schirenbeck, A., T. Bretschneider, R. Arasada, M. Schleicher, and J. Faix. 2005b. The Diaphanous-related formin dDia2 is required for the formation and maintenance of filopodia. *Nat Cell Biol*. 7:619-25.

Schoenwaelder S.M., Hughan S.C., Boniface K., Fernando S., Holdsworth M., Thompson P.E., Salem H.H., Jackson S.P. 2002 RhoA sustains integrin alpha IIbbeta 3 adhesion contacts under high shear, *J. Biol. Chem.* 277: 14738–14746.

Seth, A., Otomo, C. & Rosen, M. K. 2006 Autoinhibition regulates cellular localization and actin assembly activity of the diaphanous-related formins FRLα and mDia1. *J. Cell Biol.* **174**, 701–713

Severson, A.F., D.L. Baillie, and B. Bowerman. 2002. A Formin Homology protein and a profilin are required for cytokinesis and Arp2/3-independent assembly of cortical microfilaments in C. elegans. *Curr Biol*. 12:2066-75.

Shimada, A., M. Nyitrai, I.R. Vetter, D. Kuhlmann, B. Bugyi, S. Narumiya, M.A. Geeves, and A. Wittinghofer. 2004. The core FH2 domain of diaphanous-related

formins is an elongated actin binding protein that inhibits polymerization. *Mol Cell*. 13:511-22.

Steffen, A., J. Faix, G.P. Resch, J. Linkner, J. Wehland, J.V. Small, K. Rottner, and T.E. Stradal. 2006. Filopodia formation in the absence of functional WAVE- and Arp2/3-complexes. *Mol Biol Cell*. 17:2581-91.

Swan, K.A., A.F. Severson, J.C. Carter, P.R. Martin, H. Schnabel, R. Schnabel, and B. Bowerman. 1998. cyk-1: a C. elegans FH gene required for a late step in embryonic cytokinesis. *J Cell Sci*. 111 (Pt 14):2017-27.

Tanaka, H., E. Takasu, T. Aigaki, K. Kato, S. Hayashi, and A. Nose. 2004. Formin3 is required for assembly of the F-actin structure that mediates tracheal fusion in Drosophila. *Dev Biol*. 274:413-25.

Tolliday, N., L. VerPlank, and R. Li. 2002. Rho1 directs formin-mediated actin ring assembly during budding yeast cytokinesis. *Curr Biol*. 12:1864-70.

Tominaga, T., E. Sahai, P. Chardin, F. McCormick, S.A. Courtneidge, and A.S. Alberts. 2000. Diaphanous-related formins bridge Rho GTPase and Src tyrosine kinase signaling. *Mol Cell*. 5:13-25.

Wallar, B.J., and A.S. Alberts. 2003. The formins: active scaffolds that remodel the cytoskeleton. *Trends Cell Biol*. 13:435-46.

Wang, J., Neo, S. P. & Cai, M. 2009 Regulation of the yeast formin Bni1p by the actin-regulating kinase Prk1p. *Traffic* **10**, 528–535

Wasserman, S. 1998. FH proteins as cytoskeletal organizers. *Trends Cell Biol*. 8:111-5.

Watanabe, N., T. Kato, A. Fujita, T. Ishizaki, and S. Narumiya. 1999. Cooperation between mDia1 and ROCK in Rho-induced actin reorganization. *Nat Cell Biol*. 1:136-43.

Watanabe, N., P. Madaule, T. Reid, T. Ishizaki, G. Watanabe, A. Kakizuka, Y. Saito, K. Nakao, B.M. Jockusch, and S. Narumiya. 1997. p140mDia, a mammalian homolog of Drosophila diaphanous, is a target protein for Rho small GTPase and is a ligand for profilin. *EMBO J*. 16:3044-56.

Woychik, R.P., R.L. Maas, R. Zeller, T.F. Vogt, and P. Leder. 1990. 'Formins': proteins deduced from the alternative transcripts of the limb deformity gene. *Nature*. 346:850-3.

Xu, Y., J.B. Moseley, I. Sagot, F. Poy, D. Pellman, B.L. Goode, and M.J. Eck. 2004. Crystal structures of a Formin Homology-2 domain reveal a tethered dimer architecture. *Cell*. 116:711-23.

Young, K.G., S.F. Thurston, S. Copeland, C. Smallwood, and J.W. Copeland. 2008. Inf1 Is a Novel Microtubule-associated Formin. *Mol Biol Cell*.

Zigmond, S.H., M. Evangelista, C. Boone, C. Yang, A.C. Dar, F. Sicheri, J. Forkey, and M. Pring. 2003. Formin leaky cap allows elongation in the presence of tight capping proteins. *Curr Biol*. 13:1820-3.

Zuchero, J. B., Coutts, A. S., Quinlan, M. E., Thangue, N. B. & Mullins, R. D. 2009 p53-cofactor JMY is a multifunctional actin nucleation factor. *Nature Cell Biol.* **11**, 451–459.

Zuniga, A., O. Michos, F. Spitz, A.P. Haramis, L. Panman, A. Galli, K. Vintersten, C.

Klasen, W. Mansfield, S. Kuc, D. Duboule, R. Dono, and R. Zeller. 2004. Mouse limb deformity mutations disrupt a global control region within the large regulatory landscape required for Gremlin expression. *Genes Dev*. 18:1553-64.